Long term evolution of an escarpment in a tableland landscape (Serra Geral de Goiás, Brazil): Insights from in situ-produced cosmogenic nuclides

Luis Felipe Soares Cherem, Lionel Siame, Márcio Henrique de Campos Zancopé, Guilherme Taitson Bueno, Regis Braucher, Vincent Godard, Laëtitia Léanni, Valery Guillou, Team Aster

Graphical Abstract

Long term evolution of an escarpment in a tableland landscape (Serra Geral de Goiás, Brazil): insights from *in situ*-produced cosmogenic nuclides

Luis Felipe Soares Cherem, Lionel L. Siame, Márcio Henrique de Campos Zancopé, Guilherme Taitson Bueno, Régis Braucher, Vincent Godard, Laëtitia Leanni, Valéry Guillou, ASTER Team

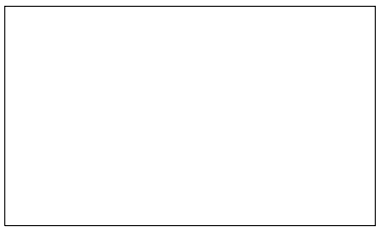

Highlights

Long term evolution of an escarpment in a tableland landscape (Serra Geral de Goiás, Brazil): insights from *in situ*-produced cosmogenic nuclides

Luis Felipe Soares Cherem, Lionel L. Siame, Márcio Henrique de Campos Zancopé, Guilherme Taitson Bueno, Régis Braucher, Vincent Godard, Laëtitia Leanni, Valéry Guillou, ASTER Team

- Complex interplay between surface processes, lithology, and climate shapes escarpments within continental interiors.
- Landslides and regolith covers significantly impact the cosmogenic signal and thus denudation rates under the secular equilibrium assumption.
- The Serra Geral Escarpment in Central Brazil has maximum rates of differential denudation and horizontal retreat of 73-81 and 30-90 m Myr^{-1}, respectively.

Long term evolution of an escarpment in a tableland landscape (Serra Geral de Goiás, Brazil): insights from *in situ*-produced cosmogenic nuclides

Luis Felipe Soares Cherem[a], Lionel L. Siame[b], Márcio Henrique de Campos Zancopé[c], Guilherme Taitson Bueno[c], Régis Braucher[b], Vincent Godard[b], Laëtitia Leanni[b], Valéry Guillou[b], ASTER Team[b,d]

[a]*Institute of Geosciences, Department of Geography, Federal University of Minas Gerais, Belo Horizonte, 31.270-901, Brazil*
[b]*Aix Marseille Univ, CNRS, IRD, INRAE, CEREGE, Aix-en-Provence, France*
[c]*Laboratory of Geomorphology, Pedology and Physical Geography (LABOGEF), Institute of Socio-Environmental Studies (IESA), Federal University of Goiás (UFG), Goiânia, 74690-900, Brazil*
[d]*Georges Aumaître, Karim Keddadouche, Fawzi Zaidi, Aix-en-Provence, France*

Abstract

Topographic escarpments are striking geomorphic features shaping the Earth's surface, often forming distinct water divides in tectonically stable regions. This study presents a new analysis of the geomorphic evolution of the Serra Geral Escarpment in the State of Goiás, Central Brazil, using *in situ*-produced cosmogenic nuclides. The objective is to quantify Quaternary denudation rates associated with different geomorphic compartments of this regional-scale escarpment by measuring the concentrations of ^{10}Be, ^{26}Al, and ^{36}Cl in river-borne sediments and bedrock outcrops. The results reveal three distinct denudation regimes: the summit surface of the Western Bahia Plateau (7.4±0.2 m Myr^{-1}), the pediplanation surface at the toe of the Serra Geral Escarpment (22.6±0.6 m Myr^{-1}), and the steep escarpment slopes (84.4±3.8 m Myr^{-1}). The significant influence of regolith burial and landslides on isotopic signatures is highlighted, underscoring the importance of accounting for these processes when interpreting cosmogenic nuclide data. Estimated escarpment retreat rates range from 30 to 90 m Myr^{-1} along active segments, while the southern region shows stabilization indicative of an advanced stage of landscape evolution. These findings demonstrate the complex interplay between geomorphic processes, lithology, and climate in shaping escarpments within continental interiors. Preliminary geomorphic evidence suggests that escarpment retreat and

pediplanation at the glint's base may have initiated as early as the upper Miocene. This study establishes a framework for understanding tropical plateau erosion and offers insights into the evolution of similar escarpments worldwide.

Keywords: Escarpment, Cosmogenic nuclides, denudation, Brazil

1. Introduction

Topographic escarpments are striking landforms that significantly influence landscape evolution. Their development is primarily governed by horizontal migration and, in the absence of tectonic forcing, is driven by surface processes controlled by climate and lithology (Heimsath et al., 2006; Godard et al., 2019). Over time, escarpments retreat horizontally, fragment into mesas and buttes, and become dissected by drainage systems (Duszyński et al., 2019).

Migoń and Duszyński (2022) highlighted the role of resistant caprock layers in preserving escarpment morphology, while the more erodible underlying strata weather and erode at a faster rate, driving parallel retreat (Twidale, 1983; Young and Wray, 2000). Groundwater seepage and sapping further accelerate this process, particularly in sedimentary scarplands, by promoting cliff undercutting and collapse (Laity and Malin, 1985; Lamb et al., 2006). These mechanisms contribute to the development of amphitheaters, scalloped escarpments, and extensive valley networks. Fracture-guided underground erosion can also lead to the gradual sagging and disintegration of caprock units (Dunne et al., 1990).

Over the past two decades, extensive research on large-scale passive margin escarpments has utilized ^{39}Ar-^{40}Ar dating of supergene oxides (Beauvais et al., 2016; Bonnet et al., 2016; Jean et al., 2020), apatite fission track analysis (Japsen et al., 2012b,a; Jelinek et al., 2014; Green et al., 2018; Jelinek et al., 2020), and (U-Th)/He thermochronology (Cockburn et al., 2000; Persano et al., 2002, 2006). Additionally, studies incorporating *in situ*-produced cosmogenic nuclides (Matmon et al., 2002; Mandal et al., 2015; Linari et al., 2017; Godard et al., 2019; Stokes et al., 2023) and numerical modeling approaches (Tucker and Slingerland, 1994; Gunnell and Fleitout, 1998; van der Beek et al., 2002; Sacek et al., 2012; Braun, 2018; Wang and Willett, 2021; Wang et al., 2021) have significantly advanced our understanding

of escarpment retreat mechanisms and rates, which can vary widely, from 1 to 10,000 m Myr^{-1}, with an average of approximately 600 m Myr^{-1} (He et al., 2024).

In Brazil, *in situ*-produced ^{10}Be concentrations in river-borne sediments have provided key insights into the geomorphic evolution of passive margin escarpments, emphasizing the roles of climate, topography, and river piracy (Salgado et al., 2016; Gonzalez et al., 2016; de Souza et al., 2019; Cherem et al., 2012; de Sordi et al., 2018). For instance, basin-wide *in situ*-produced ^{10}Be concentrations in the Serra do Mar, Southeastern Brazil, indicate denudation rates nearly half of those estimated from apatite fission track data, which suggest an average rate of roughly 50 m Myr^{-1} over the past 60 Ma (Hiruma et al., 2010; Salgado et al., 2014), indicating a decline in escarpment retreat rates since the breakup of Gondwana (*e.g.*, Hackspacher et al., 2004).

While significant research has focused on passive margin escarpments, quantitative studies on the evolution of escarpments in tableland and cuesta landscapes remain limited. (*e.g.*, Duszyński et al., 2024). In arid and semi-arid regions, studies have reported a wide range of escarpment retreat rates, with values varying from hundreds to thousands of meters per million years, influenced by factors such as climate and surface processes. In temperate regions, similar studies have shown retreat rates that vary based on local conditions, with some recent work highlighting the role of climatic and glacial-interglacial cycles in shaping escarpment dynamics (Sancho et al., 1988; Matmon et al., 2005; Duszyński et al., 2024).

Brazil is no exception, and despite its remarkable landscape diversity (Vieira et al., 2015), quantitative studies on the evolution of topographic escarpments in tableland and cuesta landscapes remain limited (Vasconcelos et al., 2019; Barreto et al., 2022). Most existing research has focused on the eastern and southeastern coast, particularly along the Atlantic Passive Margin Escarpment (see the Octopus database compiled by Codilean et al., 2022). However, recent studies have begun to explore other regions, such as the Araripe Plateau in Northeast Brazil (de Oliveira et al., 2025), expanding the scope of escarpment research in Brazil.

This study contributes to filling this gap by presenting a new dataset for one of the longest and most prominent geomorphic features in Central Brazil: the Serra Geral Escarpment,

located in the State of Goiás (Fig. 1). Our objective is to refine Quaternary denudation rates associated with different geomorphic compartments of this regional-scale escarpment by measuring the concentrations of *in situ*-produced cosmogenic nuclides (^{10}Be, ^{26}Al, and ^{36}Cl) in river-borne sediments and bedrock outcrops. These measurements offer initial constraints on the evolution of the Serra Geral Escarpment and raise broader questions about the possible impact of landslides and regolith cover on the cosmogenic signal measured in the river-borne samples.

2. Geological and geomorphic contexts

In the State of Goiás, the Serra Geral Escarpment extends along the boundary between the northwestern São Francisco Craton and the Brasília Belt, which is part of the Tocantins Province (Fig. 1) and corresponds to Early Palaeoproterozoic igneous rocks of the Transamazomic Cycle and Late Palaeoproterozoic sedimentary rocks of the Araí and Paranoá Groups, metamorphosed during the Brazilian Cycle (Schobbenhaus and Brito Neves, 2003). The São Francisco Craton is composed of Late Neoproterozoic shallow-sea sedimentary rocks from the Bambuí Group, which include clastic and carbonate-dominant formations. These are overlain by Late-Cretaceous aeolian sandstone layers of the Urucuia Group, a member of the Phanerozoic São Francisco Basin (Campos and Dardenne, 1997), establishing a stratigraphic sequence in the region. To the north, the Urucuia Group overlays Late-Palaeozoic sedimentary rocks from the Canindé Group, which belongs to the intracratonic Parnaíba Basin (Daly et al., 2019). The inclination of the Bambuí Group rocks is weak to the west, increasing to the north, with general conformity to relief and main drainage direction (Campos and Dardenne, 1997). The karst system within the Bambuí Group includes sinkholes and horizontal caves, which regulate sediment transport and water flow, playing a critical role in the regional geomorphic dynamics.

At a regional scale, the geomorphology is clearly controlled by lithostructural factors (Fig. 1). In the northwest and west, the igneous rocks correspond to a low-relief area, with elevations ranging from 250 to 350 m, known as the *Depressão do Alto Tocantins* (Upper Tocantins Depression). In the southwest, the dissected plateau has higher elevations, ranging

from 1200 to 1600 m, and is associated with Proterozoic metasedimentary rocks, forming the *Complexo Montanhoso Veadeiros-Araí* (Veadeiros-Araí Mountainous Complex, see Fig. 1).

To the east, extending from north to south, Mesozoic sandstones form a plateau with elevations between 700 and 1000 m that gently decrease eastwardly, towards the State of Bahia, known as the *Chapadão do Oeste Baiano* (Western Bahia Plateau, see Fig. 1). The central and south-central regions are characterized by low-relief areas, with elevations between 350 and 600 m, composed of limestones and calcarenites from the Bambuí Group, and known as the *Vão do Paranã* (Paranã Gap, see Fig. 1). This region exhibits an active fluvio-karst system, where chemical erosion of carbonates has created interconnected networks of caves and conduits, influencing sediment deposition and hydrology.

Between the Western Bahia Plateau and the Paranã Gap lies a narrow, N-striking, elongated intermediate surface with elevations between 750 and 800 m (Fig.1), referred to as *Patamares do Chapadão* (Plateau Steps, see Fig. 2). This surface is dissected and locally capped by pebbles, gravels and cobbles, forming a detrital paleo-pavement truncating the Lower Urucuia sandstones, the Bambuí carbonates or the Palaeoproterozoic basement rocks (Fig. 1). This regional surface likely originated through pediplanation, synchronous to the retreat of the escarpment, and was followed by fluvial dissection, bringing close to the surface the caves and caverns that developed within the limestones of the Bambuí Group (do Nascimento, 1992; Hussain and Uagoda, 2022). The Angélica fluvial cave system (Fig. 3G) is a prominent example, highlighting the interplay of vadose and phreatic processes, with sedimentary deposits reflecting episodic changes in hydrology and roof collapses.

The boundary between the Urucuia Formation and the Bambuí Group forms a major water divide between the São Francisco River to the east and the Tocantins River to the west. This divide coincides with the crest of the escarpment, which reaches an elevation of approximately 1000 m (Fig. 2). The escarpment, known as the Serra Geral de Goiás, faces westward with a vertical relief ranging from 200 to 400 m. It can be classified as a glint, similar to the topographic features like the Ibiapaba Escarpment described by Bastos et al. (2024) in Northeastern Brazil.

The Western Bahia Plateau gently dips eastward, with a poorly dissected backslope shaped by subsequent incision (Fig. 2 and 3). The surface of the plateau is covered by reddish to yellowish Oxysoils, typically thicker than 2–3 meters (Jacomine et al., 1976; Valladares, 2002), derived from the *in-situ* weathering of Urucuia sandstone throughout the Cenozoic (Kiang and de Paula, 2015). In front of the Serra Geral Escarpment, flat-topped elevations bounded by steep slopes on all sides form mesas and buttes, remnants of a once more extensive plateau. The scalloped escarpment features numerous recesses and re-entrants, separated by promontories, where regressive erosion and landslide processes have accentuated localized embayments (Fig. 2). Actually, along the whole Serra Geral Escarpment, almost 200 individual recent landslide scars were identified on Google Earth imagery, with 60% of them along the section in the region of Posse (Fig. 3).

3. Cosmogenic nuclides processing and production systematics

Cosmogenic nuclides form in surface rocks when they are bombarded by secondary cosmic particles, including neutrons and muons, triggering a series of nuclear reactions. Their accumulation is governed by the duration of exposure and the efficiency of surface processes. By analyzing rock samples, it is possible to determine denudation rates with high spatial precision, focusing on specific hillslopes or bedrock sections. Alternatively, studying amalgamated detrital sediment provides insight into the broader erosion and weathering dynamics of an entire watershed. This cosmogenic lens offers a unique perspective on surface denudation, which results from the interplay between mechanical erosion and chemical weathering.

Samples were collected during two field campaigns, one in 2017 (LFi) and the other in 2019 (LF19_i). To capture representative denudation rates reflecting regional landscape evolution, river-borne sediments were sampled from watershed outlets located across three distinct geomorphic settings (Fig. 4): on top of the Western Bahia Plateau (Chapada Group), along the Serra Geral escarpment (Escarpment Group), and at the toe of the escarpment, both before and after the karstic terrain in the Neoproterozoic limestone (Gap Group).

Additionally, surface samples were obtained from bedrock outcrops, specifically, Urucuia sandstones (LF14) and Bambuí carbonates (LF13), as well as from sandy colluvium deposits on the Plateau Steps (LF7 and LF8). All samples were processed at the *Laboratoire National des Nucléides Cosmogéniques* (LN2C, CEREGE, Aix-en-Provence, France), which houses the French AMS Facility ASTER (Arnold et al., 2010). Detailed descriptions of the chemical and AMS procedures, along with the corresponding analytical results, can be found in the supplementary materials provided in Cherem et al. (2025).

The spatial integration of cosmogenic-derived denudation rates leverages the natural mixing of sediments from slope and fluvial processes within a watershed (Brown et al., 1995; Bierman and Steig, 1996; Granger et al., 1996). As rivers transport and mix sediments originating from hillslopes, they serve as natural integrator of denudation processes across the drainage system (Von Blanckenburg, 2005). On hillslopes, cosmogenic nuclides accumulate as material moves through the upper meters of rock or regolith, recording the history of denudation and integrating both physical erosion and chemical weathering processes. If the cosmogenic nuclide concentration has reached secular equilibrium (*e.g.*, Lal, 1991) and sediment transport/storage time is negligible, the measurement of cosmogenic concentrations in river-borne quartz minerals enables estimation of basin-wide denudation rates (Granger et al., 1996; Von Blanckenburg, 2005). In this context, cosmogenic concentrations ($\bar{N}$) are inversely proportional to the long-term, basin-averaged denudation rate (ϵ):

$$\bar{N}(\epsilon) = \frac{P_n}{\lambda + \frac{\rho\epsilon}{\Lambda_n}} + \frac{P_{\mu s}}{\lambda + \frac{\rho\epsilon}{\Lambda_{\mu s}}} + \frac{P_{\mu f}}{\lambda + \frac{\rho\epsilon}{\Lambda_{\mu f}}} = \sum_i \frac{P_i}{\lambda + \frac{\rho\epsilon}{\Lambda_i}} \tag{1}$$

where λ is the radioactive decay constant of the cosmogenic nuclide (4.99×10^{-7} yr^{-1} for ^{10}Be and 9.67×10^{-7} yr^{-1} for ^{26}Al), and Λ_i represents the attenuation lengths for the cosmic particles beneath the surface. Here, the subscript i refers to the different production pathways (for ^{10}Be or ^{26}Al), including neutrons, stopping muons, and fast muons. At the watershed scale, P_i is the basin-averaged surface production rate, while ϵ is the basin-wide denudation rate. For bedrock samples, P_i is the local production rate and ϵ represents the local denudation rate. In our study, we used the attenuation lengths for neutrons (Λ_n =

150 g.cm^{-2}), slow muons ($\Lambda_{\mu s}$ = 1500 g.cm^{-2}), and fast muons ($\Lambda_{\mu f}$ = 4320 g.cm^{-2}) from Braucher et al. (2011).

To determine basin-wide surface production rates, and geomorphic shielding due to surrounding topography, scaling scheme by Stone (2000) and shielding formalism by Dunne et al. (1999) were applied to a regional digital elevation grid, extracted from the FABDEM database (Hawker et al., 2022), using in-house, Balco et al. (2008)'s MATLAB scripts and Topotoolbox (Schwanghart and Scherler, 2014). Sub-relativistic muons being sensitive only to the atmospheric thickness, their production rates are determined using the basin-averaged elevation, converted into a basin-averaged atmospheric pressure (Stone, 2000), and the formulation by Braucher et al. (2011).

In equation (1), ρ (g.cm^{-3}) is the density of the material that is exposed to secondary particles, within the upper few meters below the surface. To account for the spatial variability due to contrasting lithologies, we allowed this parameter to vary from 1.7 g.cm^{-3}, for the watersheds that drain the regolith skirting the Western Bahia Plateau, to 2.0 g.cm^{-3}, for the other watersheds draining mostly the escarpment and the Cretaceous Urucuia Formation (Costa Bomfim and Dias Gomes, 2004). Also, because the carbonates from the Bambuí Group do not comprise quartz, they do not contribute to the production of *in situ* ^{10}Be and ^{26}Al. The areas of the watersheds that are partly draining the Bambuí Group have thus being reduced to those of the quartz-bearing rocks (Fig. 4).

Equation (1) expresses cosmogenic nuclide concentrations under the assumption of a constant denudation rate over a period long enough to reach secular equilibrium. For spallogenic neutrons, this steady-state time is given by (Lal, 1991):

$$T_{\text{eff}} = \frac{1}{\lambda + \frac{\rho\epsilon}{\Lambda_n}} \tag{2}$$

However, since the different production pathways contribute independently, the total steady-state integration time is obtained by summing the reciprocals of the individual times, analogous to the addition of decay constants in parallel processes:

$$\frac{1}{T_{\text{tot}}} = \frac{1}{T_n} + \frac{1}{T_{\mu s}} + \frac{1}{T_{\mu f}} \tag{3}$$

Substituting the individual steady-state time expressions yields:

$$T_{\text{tot}} = \frac{1}{\left(\lambda + \frac{\rho\epsilon}{\Lambda_n}\right) + \left(\lambda + \frac{\rho\epsilon}{\Lambda_{\mu s}}\right) + \left(\lambda + \frac{\rho\epsilon}{\Lambda_{\mu f}}\right)} \tag{4}$$

This equation shows that the total steady-state time is determined by the sum of the contributions from neutrons and both slow and fast muons, with each process characterized by its own attenuation length and sensitivity to surface denudation. The process with the smallest time constant, *i.e.*, the term with the largest value of $\lambda + \frac{\rho\epsilon}{\Lambda_i}$, dominates the overall steady-state time.

To evaluate if surface cosmogenic production has achieved the secular equilibrium, pairing cosmogenic nuclides with different half-lives, such as ^{10}Be and ^{26}Al, has long been proposed (*e.g.,* Lal, 1991). When fluvial sediment is injected into a karst system after being exposed to cosmic particles in the source area, productions of ^{26}Al and ^{10}Be are interrupted and both nuclide initial concentrations start to decay, according to their respective radioactive half-life. In such geomorphic settings, for shielding duration exceeding roughly 200 kyr, measurements of the isotopic ratio between ^{26}Al and ^{10}Be (hereafter referred to as the Al-Be ratio) provide estimates of burial times and paleo-denudation rates (*e.g.,* Granger et al., 2013).

At the surface, for long exposure durations under a constant denudation rate above 20 m.Myr^{-1}, the Al-Be ratio is kept close to a value of 6-7 (Balco et al., 2008; Borchers et al., 2016). When denudation rates are lower than 10 m.Myr^{-1}, the nuclide ^{26}Al may reach secular equilibrium faster than ^{10}Be. Consequently, the surface Al-Be ratio can be decreased by up to 50% with respect to the surface value of 6-7 (Lal, 1991; Dunai, 2010).

In most terrestrial settings, surface denudation is higher than 10 m Myr^{-1} but apparent burial signature can still be observed in the Al-Be ratios (Struck et al., 2018). For example, transient sediment storage in the floodplain or in alluvial deposits may combine with slow transit through the river system and affect the first-order cosmogenic signal (Romans et al.,

2016; Wittmann et al., 2020; Halsted et al., 2024; de Oliveira et al., 2025). Another possibility is the decrease of the Al-Be ratios in bedrock and river-borne samples due to an accelerating denudation rate on a Pleistocene time scale (Godard et al., 2021, 2024).

In regions of low denudation rates, residence times within the production layer, comprising the regolith and saprolite, can approach the half-life of ^{26}Al and ^{10}Be, which can thus lead to substantial nuclide losses due to radioactive decay. In addition, over such long time spans, dynamic processes such as bioturbation and pedogenesis (*e.g.*, translocation of fine particles) may introduce a dynamic burial effect, which would result in sediment that are already finger-printed with depleted Al-Be ratios when they are injected into the drainage system.

To account for these complexities, we adopted the formalism proposed by Foster et al. (2015), which allows expressing ^{10}Be and ^{26}Al concentrations as a function of the mixed layer's depth (H, in meters) and the denudation rate (ε) for a steady-state mixed soil layer:

$$N = \frac{\frac{\bar{P}H}{\varepsilon\beta} + N_b}{1 + \frac{\lambda H}{\varepsilon\beta}}, \tag{5}$$

where $\bar{P}$ is the depth-averaged production rate within the soil, incorporating both spallation and muogenic production, β is the rock-to-soil density ratio, and N_b is the nuclide concentration at the bedrock-soil interface, which depends on both H and ε. Given the quartzitic nature of the bedrock, quartz enrichment processes between bedrock and soil were not considered (Foster et al., 2015). We also considered an average density of 2.4 g cm^{-3} for the sandstone from the Urucuia Formation, and 1.2 g cm^{-3} for the soil ($\beta = 2$).

In addition, bootstrapping is used to estimate the uncertainty of the mean values of ε and H by repeatedly resampling the dataset with replacement. This generates a distribution of possible outcomes, from which the standard error and confidence intervals can be determined. Bootstrapping is particularly useful when the dataset is small or when the underlying distribution is unknown, providing a robust, data-driven estimates of parameters' uncertainties.

Finally, to quantify the retreat rate (V_{retreat}) of the escarpment, we used the following

simple relationship:

$$V_{\text{retreat}} = \frac{D_{\text{escarp.}} - D_{\text{Chap.}}}{\tan \Theta} \tag{6}$$

where $D_{\text{escarp.}}$ and $D_{\text{Chap.}}$ are the denudation rates of the escarpment and the plateau, respectively, and Θ is the escarpment slope angle. This formulation assumes that the plateau slope is negligible, which is consistent with Equation 14 of Braun (2018).

4. Results

4.1. In situ-produced concentrations and denudation rates

Accelerator Mass Spectrometry results and conversion of cosmogenic concentrations into denudation rates are presented in the supplementary tables provided in Cherem et al. (2025), together with relevant information to reproduce our calculations. *In situ* ^{10}Be concentrations measured in river-borne sediment from watersheds draining the summit surface of the Western Bahia Plateau (Chapada group) are ranging from (4.0±0.1)×10^5 to (7.7±0.2)×10^5 at. g^{-1} (Fig. 5A), yielding basin-wide denudation rates ranging from 6.3±0.4 to 12.3±0.8 m Myr^{-1} (Fig. 4), with a weighted mean of 7.4±0.2 m Myr^{-1} (Fig. 5B). Samples LF1 and LF19_3 were taken from the same outlet in 2017 and 2019 and show a ^{10}Be concentration difference that is consistent with the spatial variability observed for the other samples taken from the surface of the Western Bahia Plateau.

The watersheds draining the Plateau Steps to the west (Gap Group) exhibit ^{10}Be concentrations ranging from of (1.5±0.1)×10^5 to (2.5±0.1)×10^5 at. g^{-1} (Fig. 5A), yielding denudation rates ranging from 17.2±1.2 to 28.2±1.9 m Myr^{-1} (Fig. 4), with a weighted mean of 22.6±0.6 m Myr^{-1} (Fig. 5B).

Within the Escarpment Group, the ^{10}Be concentrations measured in river-borne sediment are lower and more variable with values ranging from (1.9±0.1)×10^4 to (19.6±0.6)×10^4 at. g^{-1} (Fig. 5A), yielding denudation rates between 62.5±4.5 and 250.0±21.9 m Myr^{-1} (Fig. 3), with a weighted mean of 84.4±3.8 m Myr^{-1} (Fig. 5B). Samples LF9 and LF19_5

were taken from the same outlet in 2017 and 2019 and yielded almost identical ^{10}Be concentrations, and thus denudation rates that are not significantly different (Cherem et al., 2025).

Denudation rates derived from surface ^{10}Be concentrations in bedrock and colluvium samples are in good agreement with those from the basin-wide, river-borne sediments (Fig. 4). Indeed, sampled from the Urucuia sandstones outcropping on top of the Western Bahia Plateau, LF14 yields a surface denudation rate of 4.5±0.3 m Myr^{-1}, comparable with the lower end member of the catchment-wide denudation rates from the same geomorphic surface. Sandy samples from the Plateau Steps, at the toe of the escarpment (LF7 and LF8), yield surface denudation rates of 19.8±1.4 and 27.3±1.9 m Myr^{-1}, which are also comparable to those from the catchments draining the same geomorphic unit (Fig. 4). Finally, the sample from an outcrop of Bambuí Limestone in the Paranã Gap (LF13) shows a significantly higher denudation rate of 162.1±28.8 m Myr^{-1} (Fig. 4).

Integration time scales, calculated from equation (4) indicates that the ^{10}Be-derived denudation rates span the last 35-72 and 14-22 kyr for the Chapada and the Gap groups, respectively. For the watersheds from the Escarpment Group, the integration time scales are much shorter, and on the order of only 2-6 kyr (Cherem et al., 2025).

4.2. Al-Be ratio measurements

The ^{26}Al concentrations measured in the same samples than for the ^{10}Be concentrations, are comprised between (9.5±1.3)×10^4 and (5.6±1.9)×10^6 (Cherem et al., 2025). These concentrations yield denudation rates ranging from 8.8±0.6 to 18.3±1.3 m Myr^{-1} for the Chapada group, from 102.1±11.4 to 258.9±35.1 m Myr^{-1} for the Escarpment group, and from 21.2±1.6 to 42.7±3.0 m Myr^{-1} for the Gap group (Cherem et al., 2025). These concentrations imply Al-Be values ranging from 3.7±0.5 to 7.1±1.0. More specifically, for the Chapada Group, all the samples show low Al-Be values between 4.5±0.2 and 5.1±0.2, with a weighted mean of 4.8±0.1 (Cherem et al., 2025).

A classical means to depict cosmogenic Al-Be values is to plot them against measured ^{10}Be concentrations together with the curves drawn for the simple exposure region with

and without erosion (*e.g.,* Lal, 1991), with a normalization based on the production rate of nuclides at the sample site (Klein et al., 1986; Granger, 2006). In this graph (Fig. 5C), samples plotting along or close the "erosion island", as defined by Lal (1991), have achieved the cosmogenic secular equilibrium whereas those plotting below are characterized by complex exposure history. In the dataset, 11 out of 17 basin samples show depleted Al-Be values (30-40%), and thus plot significantly below the limiting curves (Fig. 5C).

With respect to the surface Al-Be production value of 6.61±0.52 (Rixhon et al., 2011), these samples are decreased roughly by 30%. For the Gap Group, the Al-Be values are relatively close to the theoretical surface value, with depletion below 10%, except for one sample at 30% (LF19_2). The Escarpment Group shows very variable Al-Be values, with 3 out of 5 showing depletion on the order of 36% (Cherem et al., 2025). Conversely to their ^{10}Be concentrations, samples LF9 and LF19_5 exhibit relatively different ^{26}Al concentrations. However, with a Z-score of 1.76, which is below the threshold of 1.96, these two concentrations are not significantly different at the 95% confidence level. Finally, the three bedrock samples exhibit Al-Be values close to the theoretical surface value, and thus indicate secular equilibrium.

In an attempt to estimate equivalent burial durations for the samples located in the complex exposure domain, we used the approach proposed by Blard et al. (2019). The originality of this approach lies in incorporating the effects of altitude and latitude on cosmogenic nuclide production rates, enabling more accurate burial age calculations by accounting for pre-burial exposure conditions. Apparent burial durations for the Chapada Group range from 0.4±0.1 to 0.6±0.1 Myr (Cherem et al., 2025), with a weighted mean of 0.50±0.03 Myr. For the Gap Group, burial durations are comprised between 0.2±0.1 and 0.7±0.1, for the most apparently buried sample (LF19_2, see Fig. 5C), and with a weighted mean of 0.42±0.06 Myr for the three samples with an apparent burial signature. Finally, for the watersheds in the Escarpment Group, apparent burial durations are on the order of 0.9±0.2 Myr (Cherem et al., 2025).

5. Discussion

5.1. Denudation rates and geomorphic units

Denudation rates measured from the river-borne sediments clearly separate into the three groups (Chapada, Escarpment and Gap) that were identified based on geomorphic positions and characteristics (Fig. 4). For the Chapada Group, ^{10}Be-derived denudation rates are lower than for the two other groups, with a median value of 11 m Myr^{-1}, and a weighted mean of 7.4±0.2 m Myr^{-1} (Fig. 5B). For the Escarpment Group, the ^{10}Be-derived denudation rates are higher than for the two other groups, with a median value of 160 m Myr^{-1}, and a weighted mean of 84.4±3.8 m Myr^{-1} (Fig. 5B).

Watersheds draining the Plateau Steps (Gap Group) are thus characterized by intermediate denudation rates, with a median value of 24 m Myr^{-1}, and a weighted mean of 22.6±0.6 m Myr^{-1} (Fig. 5B). Sample LF12 corresponds to a watershed that could be classified in the Escarpment Group. However, it also corresponds to the largest regional embayment that formed from regressive erosion, almost capturing the drainage network from the plateau at this latitude (Fig. 2). In this watershed, most of the slopes are close to the local base level made by the Plateau Steps, at the toe of the escarpment. For this reason, LF12 sample yields a denudation rate that is closer from those determined for the Gap Group (Fig. 4).

5.2. Interpretation of depleted Al-Be ratios

On the two-nuclides graph, the watershed samples generally plot below the curves and thus show an apparent burial signature, with very scattered samples from the Escarpment Group and more clustered samples from the Gap and Chapada groups (Fig. 4C). With the lowest ^{10}Be concentrations, samples from the escarpment are more distributed below the "erosion island" defined by the constant exposure and steady-state denudation curves (Fig. 4C). For the Escarpment Group, the observed Al-Be depletion may originate from material exposed along the escarpment slope and episodically delivered to the drainage system through landslides. In these rapidly eroding watersheds, the integration timescale of 2 to 6 kyr likely reflects the recurrence interval of gravity-driven events along this section of

the escarpment. This interpretation is reinforced by the systematic occurrence of a higher number of recent landslides in the headwaters of watersheds with the highest denudation rates (Fig. 4).

The group of river samples collected atop of the Western Bahia Plateau are characterized by low Al-Be values and high ^{10}Be concentrations. These catchments drain the flat surface of the plateau skirted by a regolith derived from the Urucuia Formation (Costa Bomfim and Dias Gomes, 2004). Before 1950 and the development of agribusiness, the Western Bahia Plateau was extensively covered by a savanna woodland (biome Cerrado), the typical natural land cover in Central Brazil. Therefore, we suspect that the depleted Al-Be results from vertical mixing under forest of the near-surface thick soil, where the combination of a strong bioturbation and slow erosion rates may have led to longer exposure, and depleted Al-Be values with respect to the surface production value (Campbell et al., 2022). Indeed, at the latitude and elevation of the Western Bahia Plateau, surface Al-Be values should be on the order of 6.4-6.8 for constant denudation rates of 5 to 13 m Myr^{-1}, as determined using ^{10}Be concentrations. However, due to the differential contributions of neutrons and muons at depth, the Al-Be values can drop by 21-27% below a ≈10 m-thick regolith with an average density of 1.7 g cm^{-3}. Conversely to the river-borne sediments, the surface sample taken from outcrop of Urucuia sandstones atop of the plateau is consistent with a long exposure at the surface with a steady denudation rate (Fig. 4C).

To explain the difference of cosmogenic signal recorded by the surface and the watershed samples, we thus invoke that the Al-Be ratios are depleted by a long exposure within the regolith that developed atop the Western Bahia Plateau. Using equation (5), ε and H were solved through an iterative optimization to match the observed concentrations of ^{10}Be and ^{26}Al (*e.g.*, Makhubela et al., 2019; Godard et al., 2024).

The ^{10}Be and ^{26}Al concentrations measured in the watersheds draining the summit surface of the Western Bahia Plateau are best explained by dynamic burial within a production layer 10.6±2.3 m thick (Fig. 6). In this framework, ε = 3.3±0.9 m Myr^{-1} represents the average basin-scale denudation rate, corrected for dynamic burial in the source production layer. Interestingly, this modeled value of ε closely aligns with the weighted mean pre-burial

erosion rates determined from the measured Al-Be ratios and the burial dating approach proposed by Blard et al. (2019). While we cannot entirely exclude the possibility of burial during sediment transport (Wittmann et al., 2020; Halsted et al., 2024), we favor the interpretation of a dynamic burial within the regolith, which acts as the source of the sampled fluvial sediments. In our dataset, the depleted Al-Be values observed for some of the watersheds from the Gap Group also suggest that this dynamic burial process may also be active within the detrital material overlaying the Plateau Steps.

The corrected denudation rate represents a conservative lower-end estimate, as our simple model does not account for quartz fractionation between the sediments of Urucuia and the regolith, nor for near-perfect vertical mixing over roughly ten meters of regolith. They are, on average, 2.5 times lower than those derived under the classical assumption of secular equilibrium. In addition, the surface sample exhibits secular equilibrium denudation rates comparable to the average basin-scale denudation rate, corrected for dynamic burial. These findings highlight the importance of considering regolith cover when deriving denudation rates from *in situ*-produced cosmogenic nuclides in river-borne sediment, as well as the potential biases introduced when relying solely on ^{10}Be concentrations and the secular equilibrium assumption.

5.3. Escarpment evolution and retreat rates

Along the northern section (LF10 and LF12) and central section (LF2, LF9, and LF_195), the escarpment displays the highest relief, with elevations reaching up to 300 meters, steep slopes exceeding 1500 m km^{-1}, and an increased number of landslides (Fig. 4). Samples from watershed outlets confined to the escarpment reveal the highest maximum denudation rates, derived from ^{10}Be concentrations, with a weighted mean of 88.5±4.0 m Myr^{-1} and a median of 168 m Myr^{-1} (Fig. 4C). These elevated rates are strongly linked to active landslides (Fig. 2), contrasting sharply with the relatively low denudation rate of 24±2 m Myr^{-1} from LF12, located in the largest embayment. The variability in Al-Be ratios highlights the stochastic nature of gravitational processes, which transport material eroded from various depths along the escarpment slopes. Indeed, high denudation rates are observed in

watersheds where landslides mobilize material from both deep and shallow sources. However, these are mainly localized adjustments, suggesting that escarpment retreat is not a uniform or rapid process but rather occurs through isolated destabilization events within a longer-term landscape adjustment.

Once embayments form and slopes stabilize, the escarpment evolution aligns with the broader regional surface at its base (*e.g.*, LF12 watershed). At this stage, denudation rates are controlled by rock outcrops as well as the availability of erodible material. Together with the gradual decline of the escarpment to the south, this might be indicative of a late-stage escarpment.

Along the southern section (LF3 and LF11), lower relief (heights below 100 meters), gentle slopes (less than 250 m km^{-1}), and less landslides suggest an advanced stage of geomorphic evolution, where slope adjustment have significantly stabilized. Al-Be ratios close to secular equilibrium and denudation rates around 30 m Myr^{-1} confirm that mass-wasting processes are less dominant. Erosion processes have stabilized across both the escarpment and adjacent headwaters, indicating a more mature landscape state.

In contrast to the northern and central sections, the southern section exhibits a higher density of karst features, such as caverns and sinkholes (see their spatial distribution in Fig. 2 and 4). This is likely due to the erosion of the Urucuia sandstones, which progressively exposes the underlying carbonate rocks of the Bambuí Group (Fig.7). Unlike fluvial incision and lateral erosion, which typically increase gravitational stresses and promote slope instability, karstification processes facilitate subsurface drainage and the gradual removal of material through dissolution. This redistribution of mass may help to mitigate gravitational stress accumulation along the escarpment face, contributing to its relative stabilization and allowing for the enhanced development of karst landforms.

The relationship between sediment transport through karst systems and depleted Al-Be ratios in downstream samples (LF19_1, LF19_2) warrants further investigation. The observed depletion in LF3 and LF11, confined to the escarpment slope, suggests that cosmic ray exposure on the slope itself may significantly contribute to the Al-Be depletion observed in some watersheds from the Gap Group (Fig. 5C).

The disparity in maximum denudation rates across the three geomorphic compartments serves as a key indicator of escarpment evolution and provides a first-order estimation of the retreat rate (Fig. 7). Mesas and buttes in the northern and central segments, alongside the Plateau Steps extending along the escarpment strike, further evidence this retreat (Fig. 2).

In the northern segment, the differential denudation between the Western Bahia Plateau (7.4±0.2 m Myr^{-1}) and the escarpment (84.4±3.8 m Myr^{-1}) is approximately 77±4 m Myr^{-1}, while in the southern segment, this difference is only 18±2 m Myr^{-1}, indicating a slower escarpment retreat (Fig. 7). Although denudation rates are expressed in terms of vertical surface lowering per unit time, their geomorphic significance differs between the plateau and the escarpment due to differences in slope angle.

On the plateau, denudation primarily reflects surface lowering through weathering and sediment transport, while on the escarpment, higher rates integrate both vertical lowering and lateral retreat. Applying equation 6, we estimated retreat rates between 30 and 90 m Myr^{-1} for Θ values ranging from 30° to 60° along the most active segments, whereas retreat in the southern segment may be up to five times slower (Fig. 6A).

Given that the Plateau Steps surface is perched approximately 200 m above the regional base level of the Paranã Gap along the central part of the escarpment (Fig. 8), and assuming that maximum denudation rates of 23±1 m Myr^{-1} (Fig. 5B), have persisted over timescales longer than the Pleistocene, we estimate that incision of the regional drainage below the Plateau Steps may have initiated at least 9.0±0.5 million years ago.

5.4. Comparison with global trends

In our dataset, the relationship between basin-wide denudation rates and mean basin slopes is weaker compared to other datasets from Brazil and worldwide (Fig. 5D). Watersheds within the Escarpment Group exhibit distinct denudation patterns that deviate from global trends. Steep escarpments are often subject to localized processes, such as landslides or episodic mass wasting, which may not be adequately captured by a simple slope-denudation relationship. Additionally, differences in sediment transport dynamics could contribute to this divergence, as escarpments may have limited sediment storage capacity, leading to

periodic pulses of sediment evacuation rather than a consistent, steady relationship with slope.

On the other hand, watersheds outside the Escarpment Group align more closely with the lower end of the global trend, indicating that their denudation rates are relatively subdued despite variations in slope. This pattern may reflect the long-term stability of the landscape, where low tectonic activity reduces the sensitivity of denudation rates to changes in slope. The weaker slope-denudation relationship in our dataset, when compared to global compilations, suggests that additional factors—such as lithology or sediment connectivity—play a more dominant role in shaping denudation rates along the Serra Geral Escarpment.

Globally, escarpment retreat rates vary widely, influenced by climate, geology, and structural characteristics. These rates span a broad range, from as low as 1 m Myr^{-1} to as high as 10,000 m Myr^{-1}, with an average retreat rate of approximately 600 m Myr^{-1} (He et al., 2024). In our study of the Serra Geral escarpment, we estimated retreat rates ranging from 30 to 90 m Myr^{-1}. These rates are relatively modest compared to those reported in other arid or semi-arid regions.

For instance, studies in Spain based on talus flatiron sequences and ^{14}C dating have found retreat rates ranging from 500 to 1050 m Myr^{-1} (Sancho et al., 1988; Gutiérrez et al., 1998; Elorza and Martínez, 2001). In the Negev Desert and the Dead Sea Basin, *in situ* ^{10}Be dating revealed rates ranging from 6-12 m Myr^{-1} to 400–700 m Myr^{-1} (Boroda et al., 2011; Matmon et al., 2005). Similarly, in temperate regions like central Queensland, Australia, and the Colorado Plateau, retreat rates have been reported between 18 and 450 m Myr^{-1} (Young and Wray, 2000; Cole and Mayer, 1982). More recently, Duszyński et al. (2024) reported retreat rates as high as 4200 m Myr^{-1} in Poland, based on ^{10}Be surface exposure dates of hillslope boulders, which advocate for variability linked to climatic and glacial-interglacial cycles.

The retreat rates we observed in the Serra Geral are on the lower end of this global spectrum, likely due to the unique climatic, lithological, and geomorphic characteristics of the region. These estimates represent maximum rates, based on cosmogenic nuclide-derived denudation under the assumption of secular equilibrium. If corrections were applied for

potential systematic Al-Be depletion, these rates could be even slower. This trend of lower retreat rates derived from cosmogenic nuclides is consistent with previous observations (e.g., Braun, 2018), where such rates are often lower than those inferred from other methods, such as thermochronology. This discrepancy likely arises from differences in integration timescales: while rates derived from cosmogenic concentrations reflect relatively recent denudation under steady-state assumptions, they do not account for longer-term escarpment dynamics, including stream piracy events and escarpment consumption. Nevertheless, our findings provide valuable insights into escarpment dynamics in tropical regions, where more resistant lithologies and relatively stable climatic conditions likely contribute to slower retreat rates compared to other regions worldwide.

6. Conclusions

This study provides an analysis of the geomorphic evolution of the Serra Geral Escarpment in Central Brazil, utilizing *in situ*-produced cosmogenic nuclides to quantify denudation rates and propose a preliminary quantification of its horizontal retreat. The key findings are:

- Distinct denudation regimes across three geomorphic units: the Chapada Group (5–13 m Myr^{-1}), the Gap Group (18–30 m Myr^{-1}), and the Escarpment Group (58–272 m Myr^{-1}).

- The influence of regolith burial and landslides on isotopic signatures. Regolith burial in the Chapada Group and deep-seated landslides in the Escarpment Group result in complex exposure histories, underscoring the importance of considering these processes when interpreting cosmogenic nuclide data.

- Significant differential denudation of about 73-81 m Myr^{-1} and escarpment retreat rates of 30–90 m Myr^{-1} along active segments. The southern region, marked by slower retreat and karstification, demonstrates stabilization indicative of advanced landscape evolution.

While isotopic data and modeling provide critical insights into the timing and rates of geomorphic processes, it is essential to recognize that progress in geomorphology depends on a holistic approach. Field verification and systematic landform mapping, whether through fieldwork or remote sensing, remain indispensable for corroborating and refining isotopic results. However, by integrating denudation rates with dynamic landscape processes, this study establishes a preliminary framework for understanding tropical plateau erosion, cuesta retreat, and offers insights into the evolution of similar escarpments worldwide.

7. Data availability

The data that support the findings of this study are openly available in DataSuds repository (IRD, France) at https://doi.org/10.23708/R4SY4X. Data reuse is granted under CC-BY license (Cherem et al., 2025).

8. Acknowledgements

The authors would like to thank the Franco-Brazilian framework for scientific collaboration (CAPES-COFECUB — projects 869/15 and 981/20) for their continuous support. We also acknowledge financial support from CNPq (462421/2014-7). Our gratitude goes to André A. Rodrigues Salgado from the Federal University of Goiás for his assistance during the initial field trip. We appreciate Piotr Migoń for his helpful comments on previous versions of the manuscript, and we also acknowledge other anonymous reviewers. The ASTER AMS national facility (CEREGE, Aix-en-Provence), supported by INSU/CNRS and IRD, is a member of the Aix-Marseille technological platforms and the REGEF network. Lionel Siame is grateful to IRD for its support through the "Mission de Longue Durée" mobility program. The authors declare no conflicts of interest relevant to this study.

References

Abbühl, L.M., Norton, K.P., Schlunegger, F., Kracht, O., Aldahan, A., Possnert, G., 2010. El niño forcing on ^{10}Be-based surface denudation rates in the northwestern peruvian andes? Geomorphology 123, 257–268.

Arnold, M., Merchel, S., Bourlès, D.L., Braucher, R., Benedetti, L., Finkel, R.C., Aumaître, G., Gottdang, A., Klein, M., 2010. The French accelerator mass spectrometry facility ASTER: Improved performance and developments. Nuclear Instruments and Methods in Physics Research, Section B: Beam Interactions with Materials and Atoms 268, 1954–1959. doi:10.1016/j.nimb.2010.02.107.

Balco, G., Stone, J., Lifton, N., Dunai, T., 2008. A complete and easily accessible means of calculating surface exposure ages or erosion rates from ^{10}Be and ^{26}Al measurements. Quaternary Geochronology 3, 174–195. doi:10.1016/j.quageo.2007.12.001.

Barreto, H.N., Braucher, R., Salgado, A.A.R., Siame, L., Léanni, L., Auler, A., Martins, F.P., Bourlès, D.L., 2022. A karstic model of the generation of tablelands landscapes in sandstones in Eastern Amazonia. J. South Am. Earth Sci. 114, 103709. doi:10.1016/j.jsames.2021.103709.

Barreto, H.N., Varajão, C.A.C., Braucher, R., Bourlès, D.L., Salgado, A.A.R., Varajão, A.F.D.C., 2013. Denudation rates of the Southern Espinhaço Range, Minas Gerais, Brazil, determined by in situ-produced cosmogenic Beryllium-10. Geomorphology 191, 1–13. doi:10.1016/j.geomorph.2013.01.021.

Bastos, F.d.H., Siame, L., Lima, D.L.d.S., Cordeiro, A.M.N., 2024. Lithostructural control of the relief in the eastern sector of the Parnaíba sedimentary basin (Ibiapaba Plateau), northeast brazil. Revista Brasileira de Geomorfologia 25, 1–24. doi:10.20502/rbgeomorfologia.v25i4.2589.

Beauvais, A., Bonnet, N.J., Chardon, D., Arnaud, N., Jayananda, M., 2016. Very long-term stability of passive margin escarpment constrained by 40Ar/39Ar dating of K-Mn oxides. Geology 44, 299–302. doi:10.1130/G37303.1.

van der Beek, P., Summerfield, M.A., Braun, J., Brown, R.W., Fleming, A., 2002. Modeling postbreakup landscape development and denudational history across the southeast African (Drakensberg Escarpment) margin. Journal of Geophysical Research: Solid Earth 107, ETG–11. doi:10.1029/2001JB000744.

Bierman, P., Steig, E.J., 1996. Estimating rates of denudation using cosmogenic isotope abundances in sediment. Earth surface processes and landforms 21, 125–139.

Blard, P.H., Lupker, M., Rousseau, M., Tesson, J., 2019. Two matlab programs for computing paleo-elevations and burial ages from paired-cosmogenic nuclides. MethodsX 6, 1547–1556. doi:10.1016/j.mex.2019.05.017.

Bonnet, N.J., Beauvais, A., Arnaud, N., Chardon, D., Jayananda, M., 2016. Cenozoic lateritic weathering and erosion history of Peninsular India from 40Ar/39Ar dating of supergene K–Mn oxides. Chemical Geology 446, 33–53. doi:10.1016/j.chemgeo.2016.04.018.

Borchers, B., Marrero, S., Balco, G., Caffee, M., Goehring, B., Lifton, N., Nishiizumi, K., Phillips, F., Schaefer, J., Stone, J., 2016. Geological calibration of spallation production rates in the cronus-earth project. Quaternary Geochronology 31, 188–198. doi:10.1016/j.quageo.2015.01.009.

Boroda, R., Amit, R., Matmon, A., Finkel, R., Porat, N., Enzel, Y., Eyal, Y., Team, A., et al., 2011.

Quaternary-scale evolution of sequences of talus flatirons in the hyperarid Negev. Geomorphology 127, 41–52.

Braucher, R., Merchel, S., Borgomano, J., Bourlès, D.L., 2011. Production of cosmogenic radionuclides at great depth: A multi element approach. Earth Planet. Sci. Lett. 309, 1–9. doi:10.1016/j.epsl.2011.06.036.

Braun, J., 2018. A review of numerical modeling studies of passive margin escarpments leading to a new analytical expression for the rate of escarpment migration velocity. Gondwana Research 53, 209–224. doi:10.1016/j.gr.2017.04.012.

Brown, E.T., Stallard, R.F., Larsen, M.C., Raisbeck, G.M., Yiou, F., 1995. Denudation rates determined from the accumulation of in situ-produced Be-10 in the Luquillo Experimental Forest, Puerto Rico. Earth and Planetary Science Letters 129, 193–202. doi:10.1016/0012-821X(94)00249-X.

Campbell, M.K., Bierman, P.R., Schmidt, A.H., Sibello Hernández, R., García-Moya, A., Corbett, L.B., Hidy, A.J., Cartas Águila, H., Guillén Arruebarrena, A., Balco, G., et al., 2022. Cosmogenic nuclide and solute flux data from central Cuban rivers emphasize the importance of both physical and chemical mass loss from tropical landscapes. Geochronology 4, 435–453. doi:10.5194/gchron-4-435-2022.

Campos, J.E.G., Dardenne, M.A., 1997. Estratigrafia e sedimentação da bacia sanfranciscana: uma revisão. Revista Brasileira de Geociências 27, 269–282.

CECAV, 2021. Cavidades Naturais Subterrâneas Brasileiras. URL: https://www.gov.br/icmbio/pt-br/assuntos/centros-de-pesquisa/cavernas.

Cherem, L.F.S., Siame, L., De Campos Zancopé, M.H., Taitson Bueno, G., Braucher, R., Godard, V., Leanni, L., Guillou, V., Team, A., 2025. Data and supplementary information for - Long term evolution of an escarpment in a tableland landscape (Serra Geral de Goiás, Brazil): insights from in situ-produced cosmogenic nuclides. URL: https://doi.org/10.23708/R4SY4X, doi:10.23708/R4SY4X.

Cherem, L.F.S., Varajão, C.A.C., Braucher, R., Bourlés, D., Salgado, A.A.R., Varajão, A.C., 2012. Long-term evolution of denudational escarpments in southeastern brazil. Geomorphology (Amst.) 173-174, 118–127. doi:10.1016/j.geomorph.2012.06.002.

Clementucci, R., Ballato, P., Siame, L., Faccenna, C., Racano, S., Torreti, G., Lanari, R., Leanni, L., Guillou, V., 2023. Transient response to changes in uplift rates in the northern Atlas-Meseta system (Morocco). Geomorphology 436, 108765. doi:10.1016/j.geomorph.2023.108765.

Cockburn, H., Brown, R., Summerfield, M., Seidl, M., 2000. Quantifying passive margin denudation and landscape development using a combined fission-track thermochronology and cosmogenic isotope analysis approach. Earth and Planetary Science Letters 179, 429–435. doi:10.1016/S0012-821X(00)00144-8.

Codilean, A.T., Munack, H., Saktura, W.M., Cohen, T.J., Jacobs, Z., Ulm, S., Hesse, P.P., Heyman, J., Peters, K.J., Williams, A.N., et al., 2022. Octopus database (v. 2). Earth System Science Data Discussions

2022, 1–30. doi:10.5194/essd-14-3695-2022.

Cole, K.L., Mayer, L., 1982. Use of packrat middens to determine rates of cliff retreat in the eastern Grand Canyon, Arizona. Geology 10, 597–599.

Costa Bomfim, L.F., Dias Gomes, R.A., 2004. Aqüífero Urucuia – geometria e espessura ideias para discussão. Reviste Águas Subterrâneas Suppl. - A, 1–9. URL: https://aguassubterraneas.abas.org/asubterraneas/article/view/23330.

do Couto, E.V., dos Santos, L.J.C., de Sordi, M.V., Bourlès, D.L., Braucher, R., Salgado, A.A.R., Léanni, L., Ferreira, J.H.D., 2018. Changes of the base levels in the Ivaí and Paraná rivers confluence zone (Southern Brazil): Denudational reflexes in the evolution of the upstream drainage network. Zeitschrift für Geomorphologie 61, 23–40. doi:10.1127/zfg/2018/0545.10.

Daly, M., Tozer, B., Watts, A., 2019. Cratonic basins and the Wilson cycle: a perspective from the parnaíba basin, Brazil. Geological Society, London, Special Publications 470, 463–477. doi:10.1144/SP470.13.

Delunel, R., van Der Beek, P.A., Carcaillet, J., Bourlès, D.L., Valla, P.G., 2010. Frost-cracking control on catchment denudation rates: Insights from in situ produced ^{10}Be concentrations in stream sediments (Ecrins–Pelvoux Massif, French Western Alps). Earth and Planetary Science Letters 293, 72–83. doi:10.1016/j.epsl.2010.02.020.

Dunai, T.J., 2010. Cosmogenic nuclides: principles, concepts and applications in the earth surface sciences. Cambridge University Press.

Dunne, J., Elmore, D., Muzikar, P., 1999. Scaling factors for the rates of production of cosmogenic nuclides for geometric shielding and attenuation at depth on sloped surfaces. Geomorphology (Amst.) 27, 3–11. doi:10.1016/S0169-555X(98)00086-5.

Dunne, T., et al., 1990. Hydrology, mechanics, and geomorphic implications of erosion by subsurface flow. Groundwater geomorphology: The role of subsurface water in earth-surface processes and landforms 252, 1–28.

Duszyński, F., Jancewicz, K., Migoń, P., Waroszewski, J., Christl, M., Tikhomirov, D., Egli, M., 2024. Changing rates of escarpment retreat linked to environmental change in a sedimentary tableland, stołowe mountains, sw poland. Geomorphology , 109314.

Duszyński, F., Migoń, P., Strzelecki, M.C., 2019. Escarpment retreat in sedimentary tablelands and cuesta landscapes–landforms, mechanisms and patterns. Earth-Science Reviews 196, 102890. doi:10.1016/j.earscirev.2019.102890.

Duxbury, J., Bierman, P.R., Portenga, E.W., Pavich, M.J., Southworth, S., Freeman, S.P., 2015. Erosion rates in and around Shenandoah National Park, Virginia, determined using analysis of cosmogenic ^{10}Be. American Journal of Science 315, 46–76. doi:10.2475/01.2015.02.

Elorza, M.G., Martínez, V.S., 2001. Multiple talus flatirons, variations of scarp retreat rates and the

evolution of slopes in Almazán Basin (semi-arid central Spain). Geomorphology 38, 19–29.

Finnegan, N.J., Hallet, B., Montgomery, D.R., Zeitler, P.K., Stone, J.O., Anders, A.M., Yuping, L., 2008. Coupling of rock uplift and river incision in the Namche Barwa–Gyala Peri massif, Tibet. Geological Society of America Bulletin 120, 142–155. doi:10.1130/B26224.1.

Foster, M.A., Anderson, R.S., Wyshnytzky, C.E., Ouimet, W.B., Dethier, D.P., 2015. Hillslope lowering rates and mobile-regolith residence times from in situ and meteoric ^{10}Be analysis, Boulder Creek Critical Zone Observatory, Colorado. Geological Society of America Bulletin 127, 862–878. doi:10/f7mv5h.

Godard, V., 2022. A set of utilities for the analysis of Terrestrial Cosmogenic Nuclides (TCN) concentrations under complex exposure and erosion histories of the Earth surface. URL: https://github.com/VincentGodard/TCNtools.

Godard, V., Dosseto, A., FLEURY, J., Bellier, O., Siame, L., Team, A., 2019. Transient landscape dynamics across the Southeastern Australian Escarpment. Earth and Planetary Science Letters 506, 397–406. doi:10.1016/j.epsl.2018.11.017.

Godard, V., Salgado, A., Siame, L., Fleury, J., Team, A., 2021. Transient hillslope erosion in slow evolution landscapes. Earth Surface Processes and Landforms 46, 2485–2500. doi:10.1002/esp.5190.

Godard, V., Siame, L.L., Salgado, A.A.R., team, A., 2024. Erosional response to Pleistocene climate changes in the Brazilian highlands. Earth Surface 129, e2024JF007671. doi:10.1029/2024JF007671.

Gomes, M.C.V., Vieira, B.C., Salgado, A.A.R., Braucher, R., 2022. Debris flow and long-term denudation rates in a tropical passive margin escarpment in south america. Geomorphology (Amst.) 413, 108333. doi:10.1016/j.geomorph.2022.108333.

Gonzalez, V.S., Bierman, P.R., Fernandes, N.F., Rood, D.H., 2016. Long-term background denudation rates of southern and southeastern brazilian watersheds estimated with cosmogenic be-10. GEOMORPHOLOGY 268, 54–63. doi:10.1016/j.geomorph.2016.05.024.

Granger, D.E., 2006. A review of burial dating methods using ^{26}Al and ^{10}Be, in: GSA Special Paper 415, L.L. Siame, D.L. Bourlès, E.T. Brown (Eds.), *In situ*-produced cosmogenic nuclides and quantification of geological processes. Geological Society of America, pp. 1–16. doi:10.1130/2006.2415(01).

Granger, D.E., Kirchner, J.W., Finkel, R., 1996. Spatially averaged long-term erosion rates measured from in situ-produced cosmogenic nuclides in alluvial sediment. The Journal of Geology 104, 249–257. doi:10.1086/629823.

Granger, D.E., Lifton, N.A., Willenbring, J.K., 2013. A cosmic trip: 25 years of cosmogenic nuclides in geology. Bulletin 125, 1379–1402. doi:10.1130/B30774.1.

Green, P.F., Japsen, P., Chalmers, J.A., Bonow, J.M., Duddy, I.R., 2018. Post-breakup burial and exhumation of passive continental margins: Seven propositions to inform geodynamic models. Gondwana Research 53, 58–81. doi:10.1016/j.gr.2017.03.007.

Gunnell, Y., Fleitout, L., 1998. Shoulder uplift of the Western Ghats passive margin, India: a denudational model. Earth Surface Processes and Landforms: The Journal of the British Geomorphological Group 23, 391–404. doi:10.1002/(SICI)1096-9837(199805)23:5<391::AID-ESP853>3.0.CO;2-5.

Gutiérrez, M., Sancho, C., Arauzo, T., 1998. Scarp retreat rates in semiarid environments from talus flatirons (Ebro Basin, NE Spain). Geomorphology 25, 111–121.

Hackspacher, P., Ribeiro, L., Ribeiro, M., Fetter, A., Neto, J.H., Tello, C., Dantas, E., 2004. Consolidation and break-up of the south american platform in southeastern Brazil: tectonothermal and denudation histories. Gondwana Research 7, 91–101.

Halsted, C., Bierman, P., Codilean, A., Corbett, L., Caffee, M., 2024. Global analysis of in situ cosmogenic $^{26}Al/^{10}Be$ ratios in fluvial sediments indicates widespread sediment storage and burial during transport. Geochronology Discussions 2024, 1–25. doi:10.5194/gchron-2024-22.

Hawker, L., Uhe, P., Paulo, L., Sosa, J., Savage, J., Sampson, C., Neal, J., 2022. A 30 m global map of elevation with forests and buildings removed. Environmental Research Letters 17, 024016. URL: https://dx.doi.org/10.1088/1748-9326/ac4d4f, doi:10.1088/1748-9326/ac4d4f.

He, C., Braun, J., Tang, H., Yuan, X., Acevedo-Trejos, E., Ott, R.F., de Quay, G.S., 2024. Drainage divide migration and implications for climate and biodiversity. Nature Reviews Earth Environment 5, 177–192. doi:10.1038/s43017-023-00511-z.

Heimsath, A.M., Chappell, J., Finkel, R.C., Fifield, K., Alimanovic, A., 2006. Escarpment erosion and landscape evolution in southeastern Australia, in: Tectonics, Climate, and Landscape Evolution. Geological Society of America, pp. 173–190. doi:10.1130/2006.2398(10).

Hiruma, S.T., Riccomini, C., Modenesi-Gauttieri, M.C., Hackspacher, P.C., Neto, J.C.H., Franco-Magalhães, A.O., 2010. Denudation history of the Bocaina Plateau, Serra do Mar, southeastern Brazil: Relationships to Gondwana breakup and passive margin development. Gondwana Research 18, 674–687.

Hussain, Y., Uagoda, R., 2022. An introduction and gis-based relief compartment mapping of fluvio-karst landscape in central Brazilian highlands. Authorea Preprints .

Insel, N., Ehlers, T.A., Schaller, M., Barnes, J.B., Tawackoli, S., Poulsen, C.J., 2010. Spatial and temporal variability in denudation across the Bolivian Andes from multiple geochronometers. Geomorphology 122, 65–77. doi:10.1016/j.geomorph.2010.05.014.

Jacomine, P.K.T., Cavalcanti, A., Ribeiro, M., Montenegro, J., Burgos, N., de Mélo Filho, H., Formiga, R., 1976. Levantamento exploratório-reconhecimento de solos da margem esquerda do Rio são Francisco Estado da Bahia.

Japsen, P., Bonow, J.M., Green, P.F., Cobbold, P.R., Chiossi, D., Lilletveit, R., Magnavita, L.P., Pedreira, A., 2012a. Episodic burial and exhumation in NE Brazil after opening of the South Atlantic. Bulletin 124, 800–816. doi:10.1130/B30515.1.

Japsen, P., Chalmers, J.A., Green, P.F., Bonow, J.M., 2012b. Elevated, passive continental margins: Not rift shoulders, but expressions of episodic, post-rift burial and exhumation. Global and Planetary Change 90, 73–86. doi:10.1016/j.gloplacha.2011.05.004.

Jean, A., Beauvais, A., Chardon, D., Arnaud, N., Jayananda, M., Mathe, P., 2020. Weathering history and landscape evolution of Western Ghats (India) from 40Ar/39Ar dating of supergene K–Mn oxides. Journal of the Geological Society 177, 523–536. doi:10.1144/jgs2019-04.

Jelinek, A., Chemale Jr, F., Van der Beek, P., Guadagnin, F., Cupertino, J., Viana, A., 2014. Denudation history and landscape evolution of the northern East-Brazilian continental margin from apatite fission-track thermochronology. Journal of South American Earth Sciences 54, 158–181. doi:10.1016/j.jsames.2014.06.001.

Jelinek, A.R., Corrêa-Gomes, L.C., Bicca, M.M., 2020. Evolução termotectônica fanerozoica da margem continental na área do Rifte Recôncavo-Tucano-Jatobá. Pesquisas em Geociências 47. doi:10.22456/1807-9806.101330.

Kiang, C.H., de Paula, F., 2015. Contribuição ao arcabouço geológico do Sistema Aquífero Urucuia. Geosciences=Geociências 34, 872–882.

Klein, J., Giegengack, R., Middleton, R., Sharma, P., Underwood, J.R., Weeks, R.A., 1986. Revealing histories of exposure using *in situ* produced ^{26}Al and ^{10}Be in Libyan Desert glass. Radiocarbon 28, 547–555. doi:10.1017/S0033822200007700.

Laity, J.E., Malin, M.C., 1985. Sapping processes and the development of theater-headed valley networks on the Colorado Plateau. Geological Society of America Bulletin 96, 203–217.

Lal, D., 1991. Cosmic ray labeling of erosion surfaces: In situ nuclide production rates and erosion models. Earth and Planetary Science Letters 104, 424–439. doi:10.1016/0012-821X(91)90220-C.

Lamb, M.P., Howard, A.D., Johnson, J., Whipple, K.X., Dietrich, W.E., Perron, J.T., 2006. Can springs cut canyons into rock? Journal of Geophysical Research: Planets 111.

Legrain, N., Stüwe, K., Wölfler, A., 2014. Incised relict landscapes in the eastern Alps. Geomorphology 221, 124–138. doi:10.1016/j.geomorph.2014.06.010.

Linari, C.L., Bierman, P.R., Portenga, E.W., Pavich, M.J., Finkel, R.C., Freeman, S.P., 2017. Rates of erosion and landscape change along the Blue Ridge escarpment, southern Appalachian Mountains, estimated from in situ cosmogenic ^{10}Be. Earth Surface Processes and Landforms 42, 928–940. doi:10.1002/esp.4051.

Makhubela, T., Kramers, J., Scherler, D., Wittmann, H., Dirks, P., Winkler, S., 2019. Effects of long soil surface residence times on apparent cosmogenic nuclide denudation rates and burial ages in the Cradle of Humankind, South Africa. Earth Surface Processes and Landforms 44, 2968–2981. URL: https://onlinelibrary.wiley.com/doi/abs/10.1002/esp.4723, doi:10/gg5s2s.

Mandal, S.K., Lupker, M., Burg, J.P., Valla, P.G., Haghipour, N., Christl, M., 2015. Spatial variability of ^{10}Be-derived erosion rates across the southern Peninsular Indian escarpment: A key to landscape evolution across passive margins. Earth and Planetary Science Letters 425, 154–167. doi:10.1016/j.epsl.2015.05.050.

Matmon, A., Bierman, P., Enzel, Y., 2002. Pattern and tempo of great escarpment erosion. Geology 30, 1135–1138. doi:10.1130/0091-7613(2002)030<1135:PATOGE>2.0.CO;2.

Matmon, A., Bierman, P., Larsen, J., Southworth, S., Pavich, M., Caffee, M., 2003. Temporally and spatially uniform rates of erosion in the southern Appalachian Great Smoky Mountains. Geology 31, 155–158. doi:10.1130/0091-7613(2003)031<0155:TASURO>2.0.CO;2.

Matmon, A., Shaked, Y., Porat, N., Enzel, Y., Finkel, R., Lifton, N., Boaretto, E., Agnon, A., 2005. Landscape development in an hyperarid sandstone environment along the margins of the Dead Sea fault: Implications from dated rock falls. Earth and Planetary Science Letters 240, 803–817.

Migoń, P., Duszyński, F., 2022. Landscapes and landforms in coarse clastic sedimentary tablelands–is there a unifying theme? Catena 218, 106545.

Miller, S.R., Sak, P.B., Kirby, E., Bierman, P.R., 2013. Neogene rejuvenation of central Appalachian topography: Evidence for differential rock uplift from stream profiles and erosion rates. Earth and Planetary Science Letters 369, 1–12. doi:10.1016/j.epsl.2013.04.007.

do Nascimento, M.A.L., 1992. Geomorfologia do estado de goiás. Boletim Goiano de Geografia 12, 01–22.

Norton, K.P., Vanacker, V., 2009. Effects of terrain smoothing on topographic shielding correction factors for cosmogenic nuclide-derived estimates of basin-averaged denudation rates. Earth Surface Processes and Landforms 34, 145–154. doi:10.1002/esp.1700.

de Oliveira, J.G., Siame, L.L., Santos, L.J.C., Leanni, L., Ribeiro, S.C., Bastos, F.d.H., ASTER Team, 2025. Relief inversion and denudation dynamics in a semi-arid landscape (Araripe Plateau, NE Brazil): Insights from cosmogenic nuclides and geomorphic surfaces. Submitted to Evolving Earth .

Ouimet, W.B., Whipple, K.X., Granger, D.E., 2009. Beyond threshold hillslopes: Channel adjustment to base-level fall in tectonically active mountain ranges. Geology 37, 579–582. doi:10.1130/G30013A.1.

Persano, C., Bishop, P., Stuart, F., 2006. Apatite (U–Th)/He age constraints on the Mesozoic and Cenozoic evolution of the Bathurst region, New South Wales: evidence for antiquity of the continental drainage divide along a passive margin. Australian Journal of Earth Sciences 53, 1041–1050. doi:10.1080/08120090600923303.

Persano, C., Stuart, F.M., Bishop, P., Barfod, D.N., 2002. Apatite (U–Th)/He age constraints on the development of the Great Escarpment on the southeastern Australian passive margin. Earth and Planetary Science Letters 200, 79–90. doi:10.1016/S0012-821X(02)00614-3.

Rezende, É.A., Salgado, A.A.R., da Silva, J.R., Bourlès, D., Braucher, R., Léanni, L., 2013. Fatores

804 Controladores da Evolução do Relevo no Flanco NNW do Rift Continental do Sudeste do Brasil: Uma
805 Análise Baseada na Mensuração dos Processos Denudacionais de Longo-termo. Revista Brasileira de
806 Geomorfologia 14. doi:10.20502/rbg.v14i2.416.
807 Rixhon, G., Braucher, R., Bourlès, D., Siame, L., Bovy, B., Demoulin, A., 2011. Quaternary river incision
808 in NE Ardennes (Belgium)-insights from ^{10}Be/^{26}Al dating of river terraces. Quaternary Geochronology
809 6, 273–284. doi:10.1016/j.quageo.2010.11.001.
810 Romans, B.W., Castelltort, S., Covault, J.A., Fildani, A., Walsh, J., 2016. Environmental signal propagation
811 in sedimentary systems across timescales. Earth-Science Reviews 153, 7–29. doi:10.1016/j.earscirev.
812 2015.07.012.
813 Sacek, V., Braun, J., Van Der Beek, P., 2012. The influence of rifting on escarpment migration on high
814 elevation passive continental margins. Journal of Geophysical Research: Solid Earth 117. doi:10.1029/
815 2011JB008547.
816 Safran, E.B., Bierman, P.R., Aalto, R., Dunne, T., Whipple, K.X., Caffee, M., 2005. Erosion rates driven
817 by channel network incision in the Bolivian Andes. Earth Surface Processes and Landforms: The Journal
818 of the British Geomorphological Research Group 30, 1007–1024. doi:10.1002/esp.1259.
819 Salgado, A., Varajão, C., Colin, F., Braucher, R., Varajão, A., Nalini, Jr, H., 2007. Study of the erosion rates
820 in the upper Maracujá Basin (Quadrilátero Ferrífero/MG, Brazil) by the in situ produced cosmogenic
821 ^{10}Be method. Earth Surf. Process. 32, 905–911. doi:10.1002/esp.1448.
822 Salgado, A.A., Marent, B.R., Cherem, L.F., Bourlès, D., Santos, L.J., Braucher, R., Barreto, H.N., 2014.
823 Denudation and retreat of the Serra do Mar escarpment in southern brazil derived from in situ-produced
824 10be concentration in river sediment. Earth Surface Processes and Landforms 39, 311–319.
825 Salgado, A.A.R., de Andrade Rezende, E., Bourles, D., Braucher, R., Da Silva, J.R., Garcia, R.A., 2016.
826 Relief evolution of the continental rift of southeast brazil revealed by in situ-produced ^{10}Be concentrations
827 in river-borne sediments. Journal of South American Earth Sciences 67, 89–99. doi:10.1016/j.jsames.
828 2016.02.002.
829 Sancho, C., Gutiérrez, M., Peña, J., Burillo, F., 1988. A quantitative approach to scarp retreat starting
830 from triangular slope facets (Central Ebro Basin, Spain). Catena supplement 13, 139–146.
831 Scharf, T.E., Codilean, A.T., De Wit, M., Jansen, J.D., Kubik, P.W., 2013. Strong rocks sustain ancient
832 postorogenic topography in southern Africa. Geology 41, 331–334. doi:10.1130/G33806.1.
833 Schobbenhaus, C., Brito Neves, B.B.d., 2003. A geologia do brasil no contexto da plataforma sul-americana.
834 Geologia, Tectônica e Recursos Minerais do Brasil. Brasília, CPRM , 5–25.
835 Schwanghart, W., Scherler, D., 2014. Short communication: Topotoolbox 2 – matlab-based software for
836 topographic analysis and modeling in earth surface sciences. Earth Surface Dynamics 2, 1–7. doi:10.
837 5194/esurf-2-1-2014.

Siame, L.L., Espíndola Rosa, L., Soares Cherem, L.F., Guilherme de Oliveira, J., Evrard, O., Barhoumi, H., Leanni, L., Duvivier, A., Blard, P.H., Bourlès, D.L., ASTER Team, Cornu, S., 2023. Natural denudation versus anthropogenically accelerated erosion in central Brazil: A confrontation of time and space scales. Earths Future 11. doi:10.1029/2022EF0032973.

de Sordi, M.V., Salgado, A.A.R., Siame, L., Bourlès, D., Paisani, J.C., Léanni, L., Braucher, R., Do Couto, E.V., Team, A., et al., 2018. Implications of drainage rearrangement for passive margin escarpment evolution in southern Brazil. Geomorphology 306, 155–169. doi:10.1016/j.geomorph.2018.01.00.

de Souza, D.H., Stuart, F.M., Rodés, Á., Pupim, F.N., Hackspacher, P.C., 2019. Controls on the erosion of the continental margin of southeast brazil from cosmogenic ^{10}Be in river sediments. Geomorphology (Amst.) 330, 163–176. doi:10.1016/j.geomorph.2019.01.020.

Stokes, M.F., Larsen, I.J., Goldberg, S.L., McCoy, S.W., Prince, P.P., Perron, J.T., 2023. The erosional signature of drainage divide motion along the blue ridge escarpment. Journal of Geophysical Research: Earth Surface 128. doi:10.1029/2022JF006757.

Stone, J.O., 2000. Air pressure and cosmogenic isotope production. J. Geophys. Res. 105, 23753–23759. doi:10.1029/2000JB900181.

Struck, M., Jansen, J.D., Fujioka, T., Codilean, A.T., Fink, D., Fülöp, R.H., Wilcken, K.M., Price, D.M., Kotevski, S., Fifield, L.K., Chappell, J., 2018. Tracking the ^{10}Be-^{26}Al source-area signal in sediment-routing systems of arid central Australia. Earth Surface Dynamics 6, 329–349. doi:10.5194/esurf-6-329-2018.

Tucker, G.E., Slingerland, R.L., 1994. Erosional dynamics, flexural isostasy, and long-lived escarpments: A numerical modeling study. Journal of Geophysical Research: Solid Earth 99, 12229–12243. doi:10.1029/94JB00320.

Twidale, C., 1983. Slope processes active late in arid scarp retreat. Zeitschrift fur Geomorphologie 27, 343–361.

Valladares, G.S., 2002. Caracterização dos solos e classes de terra para irrigaação do Oeste da Bahia - Documentos 19. Technical Report. Embrapa Monitoramento por Satélite. Campinas. URL: https://www.infoteca.cnptia.embrapa.br/bitstream/doc/16805/4/d19caractsolosba.pdf.

Vanacker, V., von Blanckenburg, F., Hewawasam, T., Kubik, P., 2007. Constraining landscape development of the Sri Lankan escarpment with cosmogenic nuclides in river sediment. Earth and Planetary Science Letters 253, 402–414. doi:10.1016/j.epsl.2006.11.003.

Varajão, C.A.C., de Alkmim, F.F., Braucher, R., Endo, I., Cherem, L.F.S., Salgado, A.A.R., Varajão, A.F.D.C., 2018. Denudation rates in the Pancas Bornhardt Province (SE Brazil), inferred from in situ produced cosmogenic ^{10}Be. Z. Geomorphol. Suppl. Issues 62, 13–22. doi:10.1127/zfg/2018/0496.

Vasconcelos, P.M., Farley, K.A., Stone, J., Piacentini, T., Fifield, L.K., 2019. Stranded landscapes in

872 the humid tropics: Earth's oldest land surfaces. Earth and Planetary Science Letters 519, 152–164.
873 doi:10.1016/j.epsl.2019.04.014.
874 Vieira, B.C., Salgado, A.A.R., Santos, L.J.C., 2015. Landscapes and landforms of Brazil. Springer.
875 Von Blanckenburg, F., 2005. The control mechanisms of erosion and weathering at basin scale from cos-
876 mogenic nuclides in river sediment. Earth and Planetary Science Letters 237, 462–479. doi:10.1016/j.
877 epsl.2005.06.030.
878 Wang, Y., Willett, S., 2021. Escarpment retreat rates derived from detrital cosmogenic nuclide concentra-
879 tions. Earth Surface Dynamics Discussions 2021, 1–38.
880 Wang, Y., Willett, S.D., Wu, D., Haghipour, N., Christl, M., 2021. Retreat of the great escarpment of
881 madagascar from geomorphic analysis and cosmogenic 10be concentrations. Geochemistry, Geophysics,
882 Geosystems 22, e2021GC009979. doi:10.5194/esurf-9-1301-2021.
883 Wittmann, H., von Blanckenburg, F., Kruesmann, T., Norton, K.P., Kubik, P.W., 2007. Relation between
884 rock uplift and denudation from cosmogenic nuclides in river sediment in the Central Alps of Switzerland.
885 Journal of Geophysical Research: Earth Surface 112. doi:10.1029/2006JF000729.
886 Wittmann, H., Oelze, M., Gaillardet, J., Garzanti, E., von Blanckenburg, F., 2020. A global rate of
887 denudation from cosmogenic nuclides in the Earth's largest rivers. Earth-Science Reviews 204, 103147.
888 doi:10.1016/j.earscirev.2020.103147.
889 Young, R., Wray, R., 2000. Contribution to the theory of scarpland development from observations in central
890 Queensland, Australia. The Journal of Geology 108, 705–719.

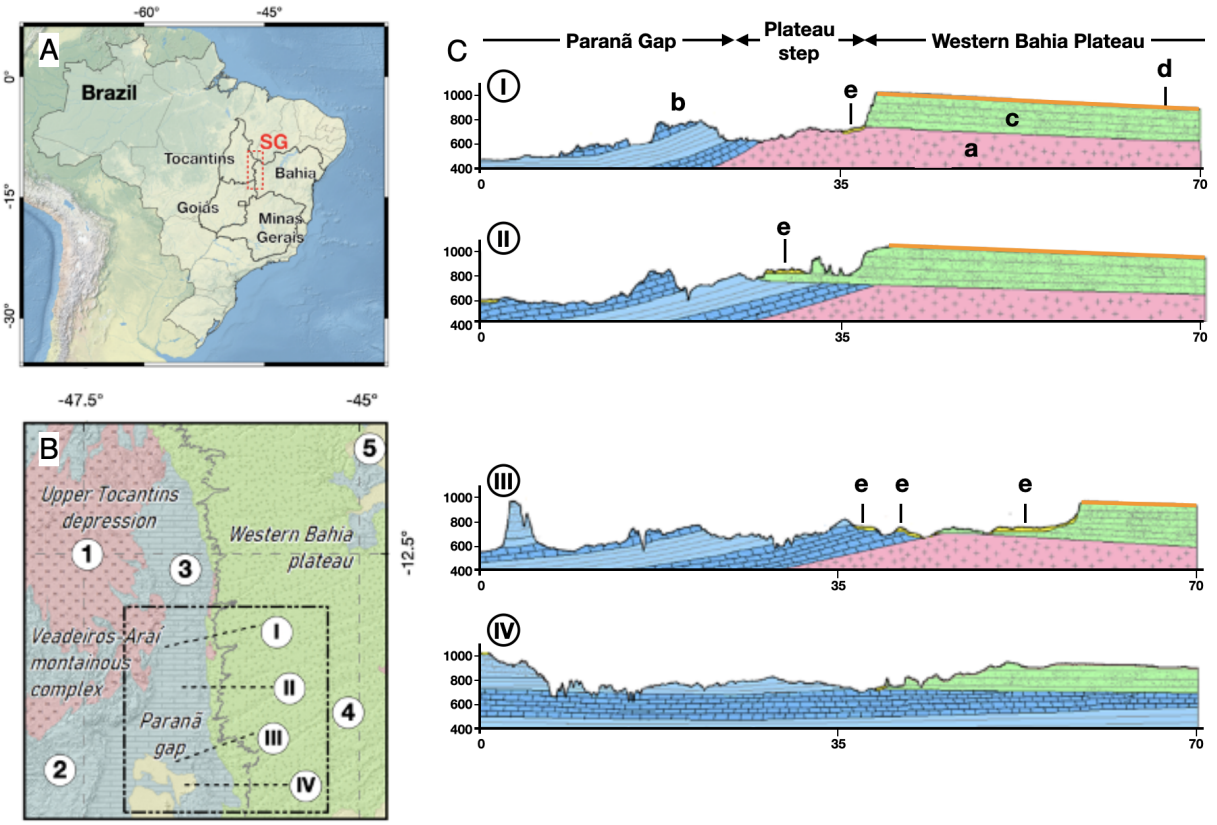

Figure 1: Location of the Serra Geral Escarpment in Brazil. A. General localization in Brazil (SG: Serra Geral). B. Main geological units of the studied area and localization of the geological cross sections (I to IV): (1) Palaeoproterozoic granitoids of Natividade Unit, and orthogneisses of Almas Cavalcante Unit, and metapelites of Arraias Formation; (2) Mesoproterozoic metasedimentary rocks of Paranoá Group; (3) Neoproterozoic sedimentary rocks of Bambuí Group; (4) Cretaceous sandstones of Urucuia Group; (5) Tertiary and Quaternary unconsolidated sediments and surficial covers. D. Sketch geological profiles centered along the Serra Geral Escarpment, identified as I, II, III, and IV, accordingly to their locations plotted in the map shown in C. These profiles also locate the main geomorphic units: Paranã Gap, Plateau Step, and Western Bahia Plateau. keys: (a) Palaeoproterozoic basement; (b) Neoproterozoic sedimentary rocks of Bambuí Group; (c) Cretaceous sandstones of Urucuia Group; (d) Laterite cover; (e) alluvial cover.

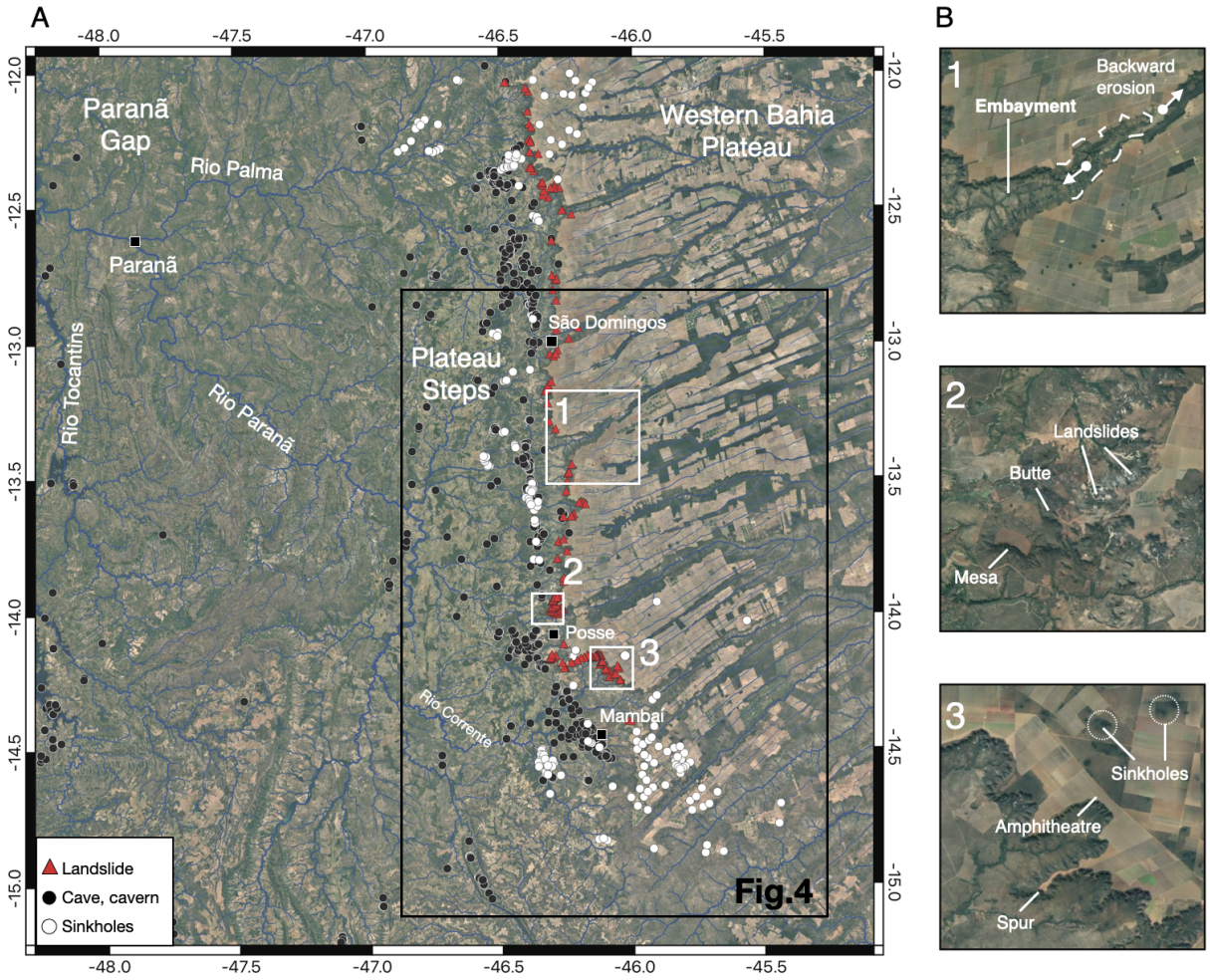

Figure 2: Geomorphic characteristics of the Serra Geral Escarpment. A. Satellite image centered on the studied section of the escarpment (Source of images: © CNES/Airbus, Google), showing the general morphology with the strong contrast of land use between the surface of the plateau (Western Bahia Plateau) and that of the depression (Paranã Gap). Distribution of caves and caverns is from *Centro Nacional de Pesquisas e Conservação de Cavernas* (CECAV, 2021). Sinkhole and landslide positions were manually extracted from satellite imagery on Google Earth. B. Enlargements of the satellite image for selected areas, showing the main geomorphic features of the escarpment: amphitheaters and embayments with backward erosion, buttes, mesas, and sinkholes (on the plateau).

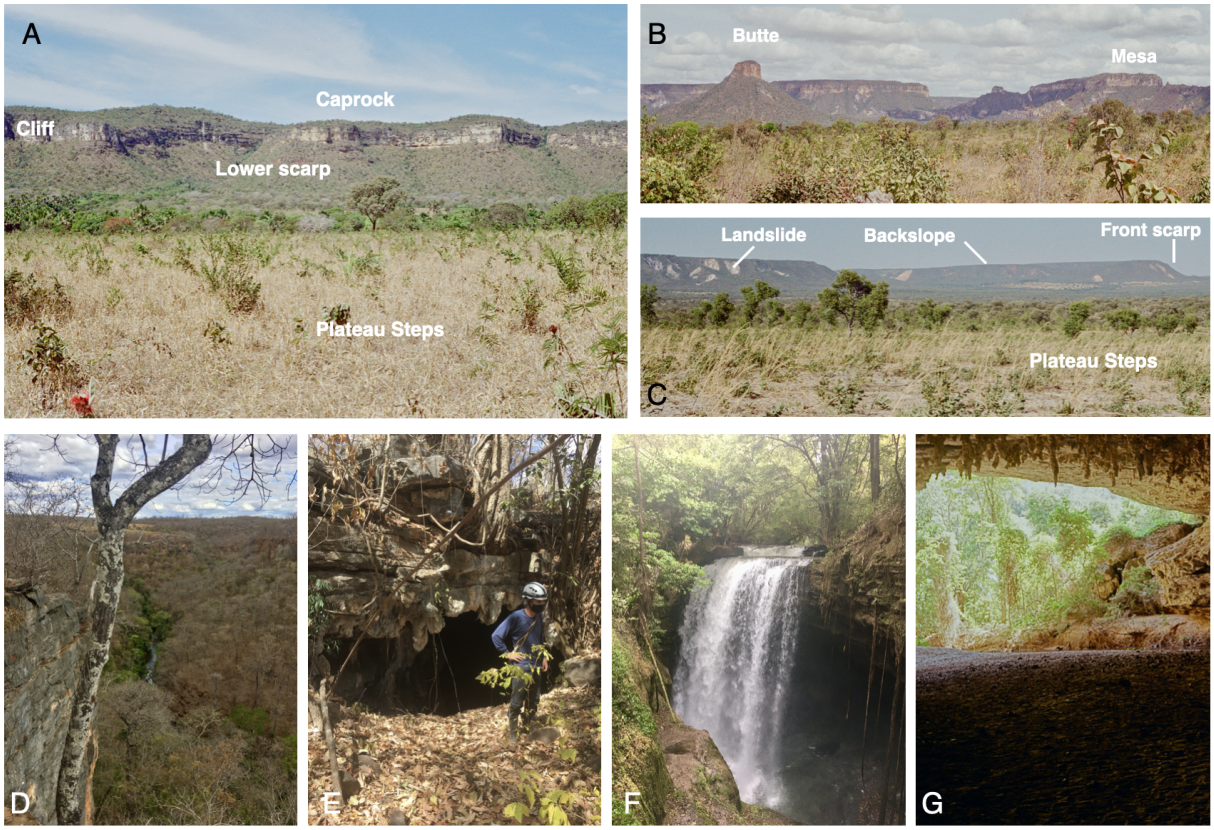

Figure 3: Field photographs illustrating the geomorphic characteristics of the Serra Geral Escarpment. A-C, General views from the Plateau Steps, showing the prominent cliff sustained by the Urucuia sandstones (caprock) above the lower scarp. The underlying, more erodible strata weather and erode at a faster rate, driving the parallel retreat of the escarpment. Along the escarpment, buttes and mesas—remnants of a once more extensive plateau—are common features. Landslides are frequently observed, indicating active slope instability and ongoing erosional processes. (D–G) Examples of regional fluvio-karst features sculpted in the Bambuí limestones and exposed by escarpment retreat. (D) Rio Corrente entrenched within its canyon. (E) A cave entrance. (F) A waterfall plunging into a cavern (Cachoeira do Funil, Mambaí, Goiás). (G) A large cavern entrance near Mambaí, highlighting the extensive subterranean drainage network (Caverna Angélica, Parque Estadual Terra Ronca, Goiás).

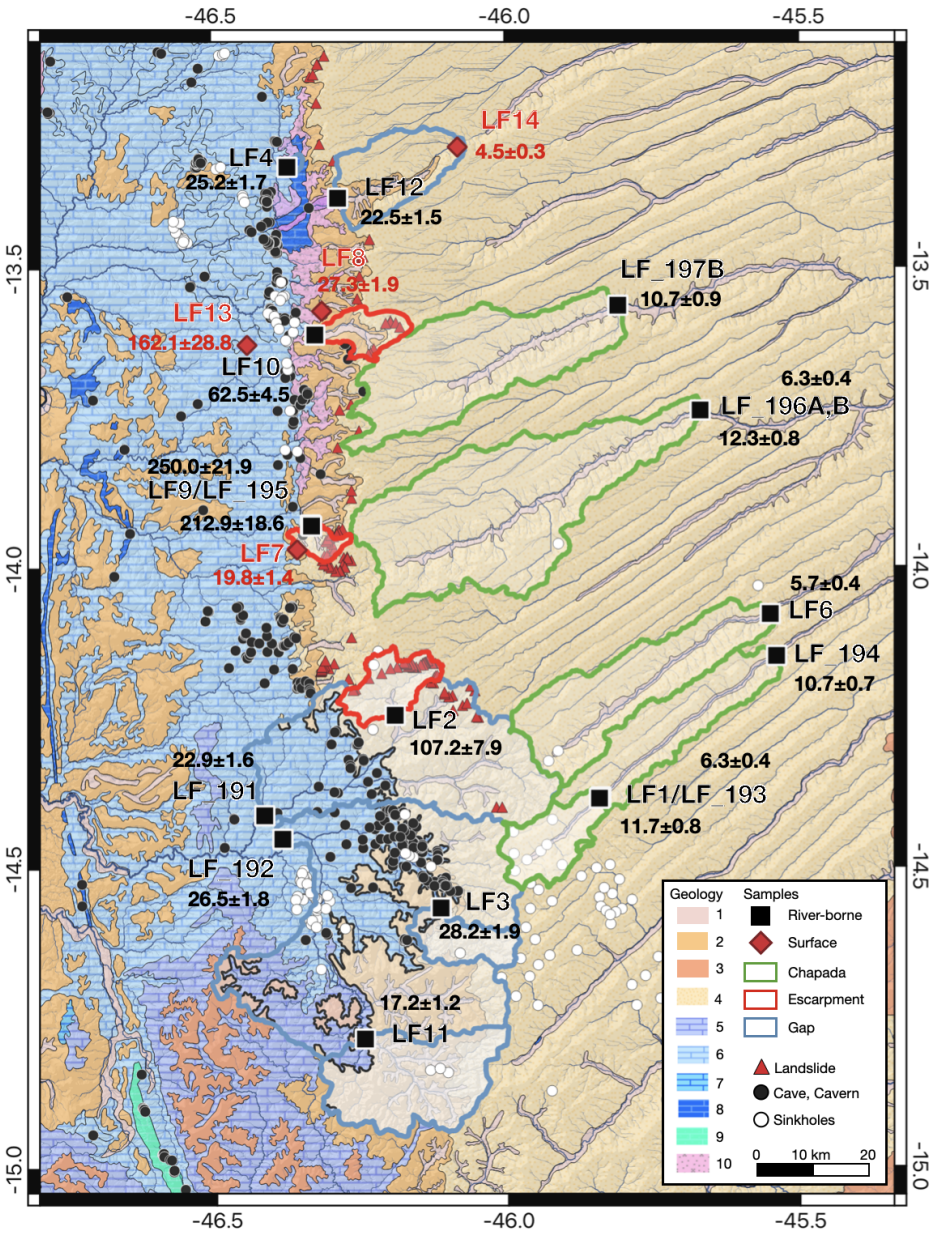

Figure 4: Localization map of cosmogenic nuclide samples and associated denudation rates along the studied segment of the Serra Geral Escarpment. Red diamonds and black squares locate surface samples on bedrock and colluvium surfaces, and river-borne sands, respectively. Polygons delimit watersheds selected on the top of the plateau (Chapada group, green), at the toe of the escarpment (Escarpment group, red) and downstream of the Plateau Steps (Gap Group, blue). All values are given in m Myr^{-1}, and correspond to *in situ*-produced ^{10}Be derived denudation rates (secular equilibrium hypothesis), excepted for LF13 that used *in situ*-produced ^{36}Cl (Cherem et al., 2025). Keys: 1, Alluvial deposits (Holocene); 2, Detrital-laterite cover (Pleistocene); 3, Detrital-lateritic cover (Paleogene); 4, Sandstone (Urucuia Group, Cretaceous); 5-8, Carbonate (Bambuí Group: 5, Três Marias; 6, Paraopeba; 7, Lagoa do Jacaré; 8, Sete Lagoas); 9, metasedimentary carbonate-pelite sequences (Paranoá Group, Palaeoproterozoic); 10, orthogneiss (Alma Cavalcante, Palaeoproterozoic). Landslides, caves and sinkholes: same as Fig. 2.

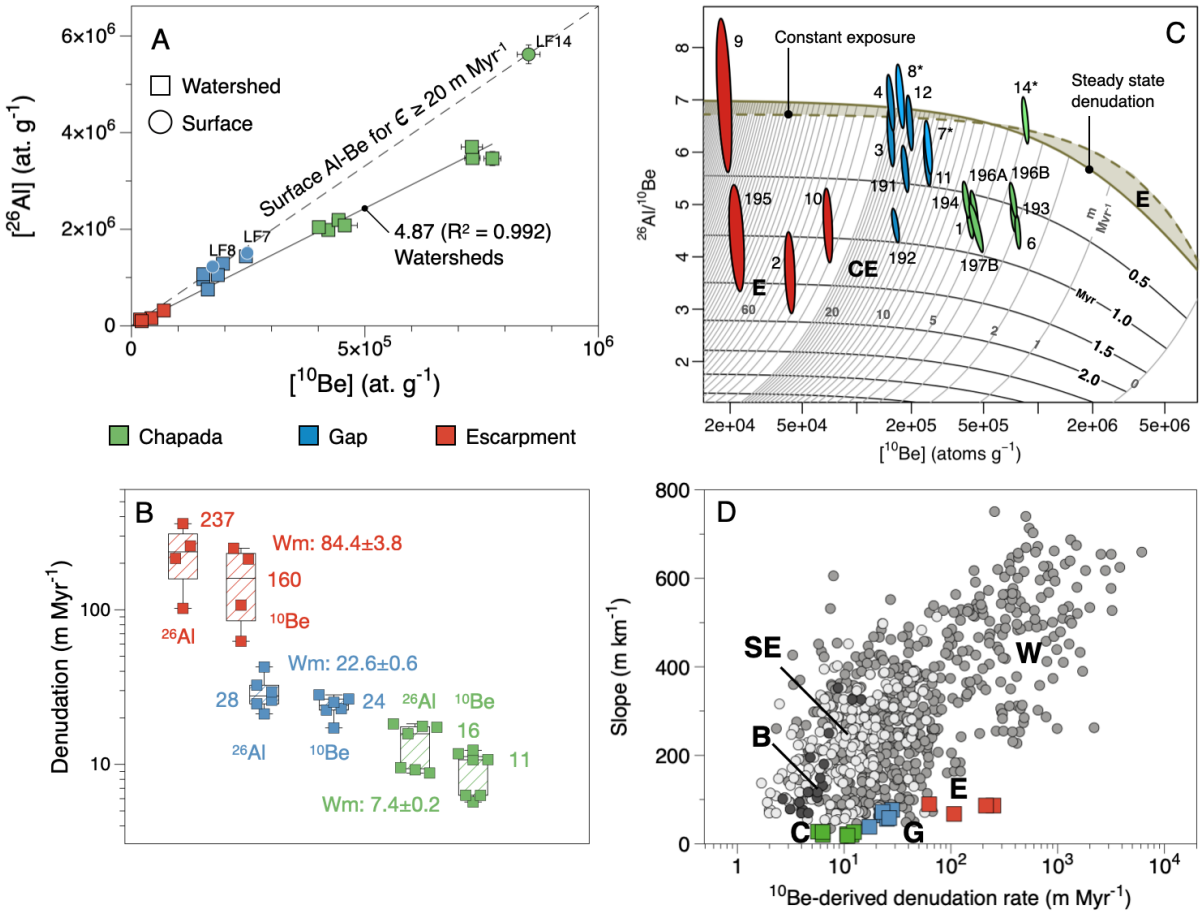

Figure 5: Results for *in situ*-produced cosmogenic concentrations. A. ^{26}Al as a function of ^{10}Be concentrations for the three watershed groups and surface samples. Dotted line: surface Al-Be ratio for denudation rates above 20 m Myr^{-1}. Plain line: forced to origin regression for the watershed samples. B. Whisker boxes with median values for ^{26}Al and ^{10}Be-derived denudation rates (m Myr^{-1}), for the three groups of watershed samples. C. Two-nuclides plot for the three groups of watershed and surface samples. Surface samples, shown in lighter colors and marked by a star, plot along the erosion island as defined by Lal (1991). This plot was elaborated using the R package *TCNtools* by Godard (2022). D. Slope (m km^{-1}) – Denudation (m Myr^{-1}) relationship. The data from Serra Geral de Goiás (E, Escarpment; G, Gap; C, Chapada) are compared to data from Brasília (B; Siame et al., 2023), Southeastern Brazil (SE; Salgado et al., 2007; Cherem et al., 2012; Barreto et al., 2013; Rezende et al., 2013; Gonzalez et al., 2016; Salgado et al., 2014, 2016; do Couto et al., 2018; Varajão et al., 2018; de Sordi et al., 2018; de Souza et al., 2019; Gomes et al., 2022), and the rest of the world (W; Matmon et al., 2003; Safran et al., 2005; Wittmann et al., 2007; Vanacker et al., 2007; Finnegan et al., 2008; Norton and Vanacker, 2009; Ouimet et al., 2009; Delunel et al., 2010; Abbühl et al., 2010; Insel et al., 2010; Miller et al., 2013; Scharf et al., 2013; Legrain et al., 2014; Duxbury et al., 2015; Mandal et al., 2015; Godard et al., 2019; Clementucci et al., 2023).

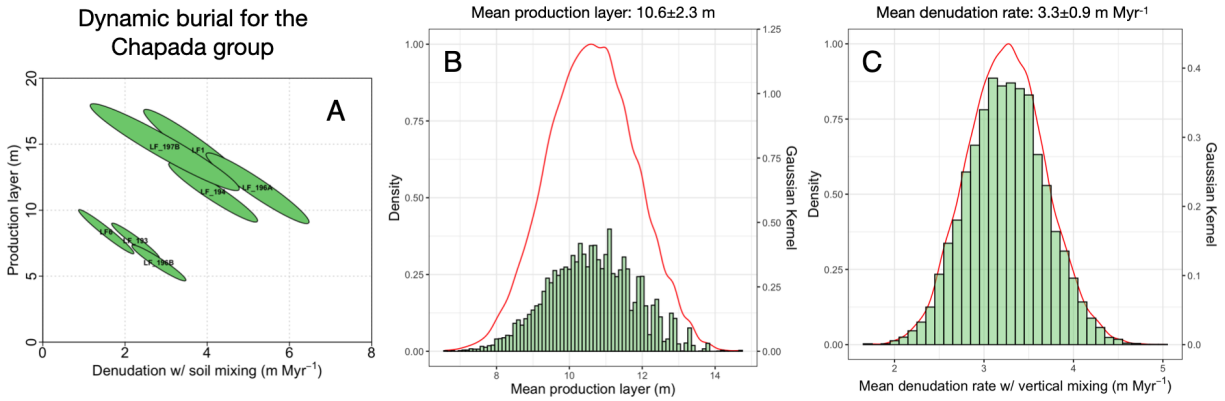

Figure 6: Results for the dynamic burial model applied to the river-borne samples from the Chapada group. A. Production layer thickness (m) as a function the denudation with burial mixing (m Myr^{-1}) for each sample from the Chapada Group, with 1σ confidence ellipses. B. and C. Probability density functions for the bootstrapped mean production layer depths and denudation rates with burial mixing, with Gaussian kernel smoothing and histogram overlays. This model and plots were elaborated using the R package *TCNtools* by Godard (2022).

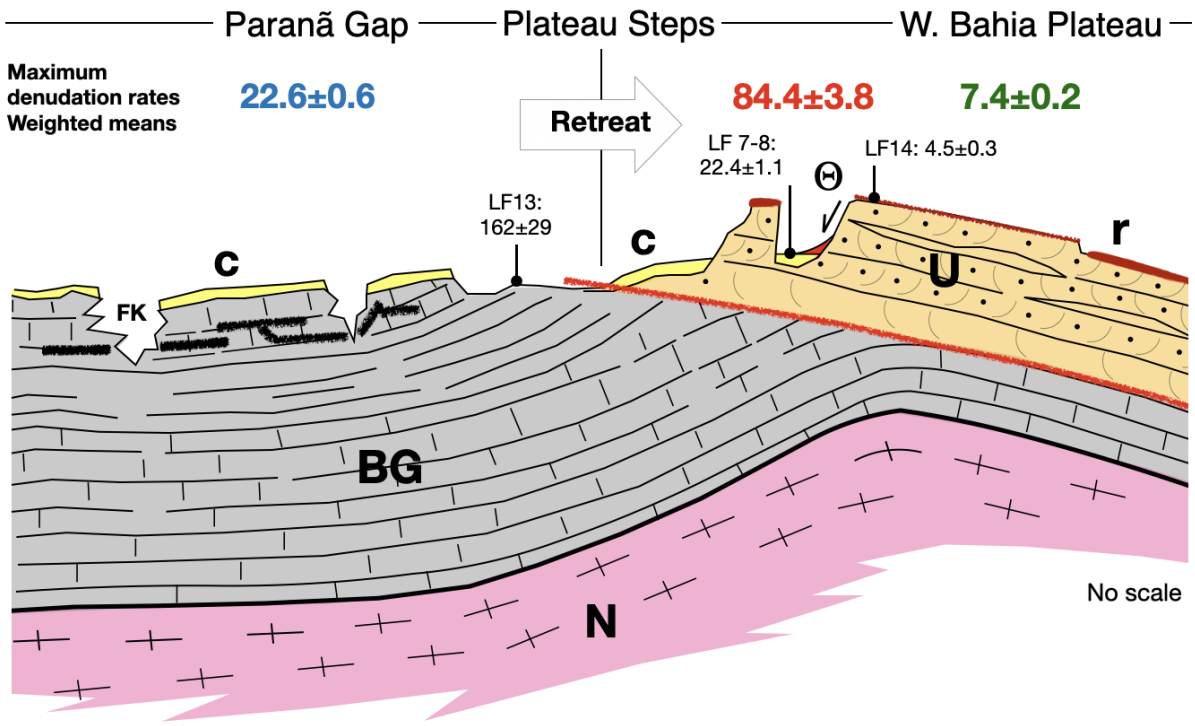

Figure 7: Schematic cross-section of the studied escarpment section with the weighted mean values for ^{10}Be-derived denudation rates (in m Myr^{-1}). Surface samples are approximately localized along the cross-section. Dark thick lines indicate the cave network connected to the fluvio-karst. Red thick line underlines the unconformity between Urucuia and Bambuí groups. Keys: FK, fluvio-karst; c, colluvial material skirting the Plateau Steps; r, regolith skirting the Western Bahia Plateau; U, Urucuia Formation; BG, Bambuí Group; N, Neoproterozoic basement.

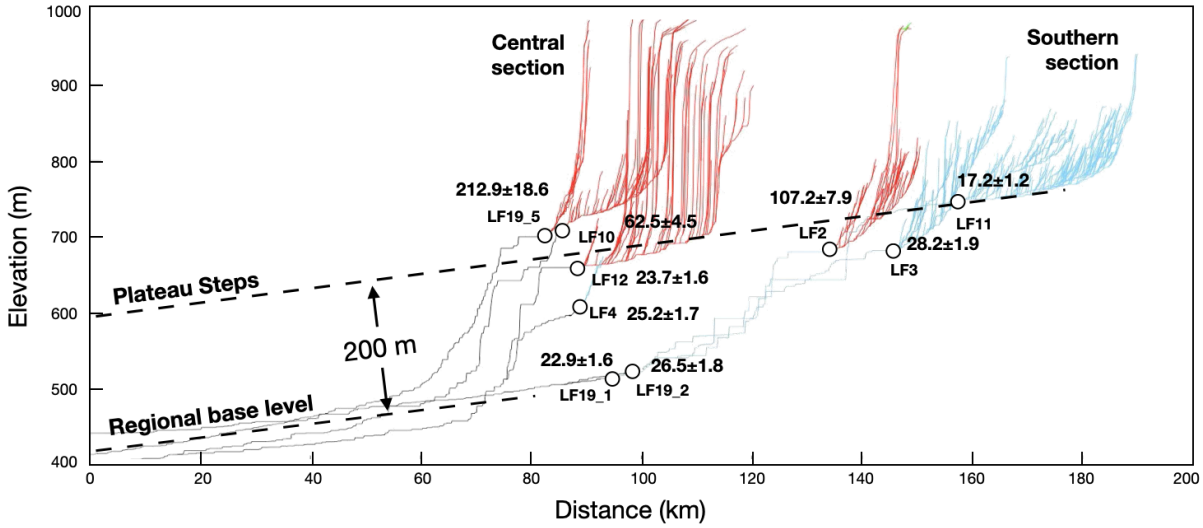

Figure 8: River profiles with all the sampled outlets and maximum, basin-wide denudation rates determined using ^{10}Be concentrations. Dotted lines indicate vertical position of the Plateau steps with respect to the regional base level. Red and blue lines indicate individual river profiles for the central and the southern section of the Serra Geral Escarpment, respectively.